FGF/MAPK signaling sets the switching threshold of a mutual repressor circuit controlling cell fate decisions in ES cells

Christian Schröter, Pau Rué, Jonathan P. Mackenzie and Alfonso Martinez Arias

Department of Genetics, University of Cambridge, Downing Street, Cambridge CB2 3EH, United Kingdom

Correspondence: cs684@cam.ac.uk; ama11@cam.ac.uk

Abstract

Intracellular transcriptional regulators and extracellular signaling pathways together regulate the allocation of cell fates during development, but how their molecular activities are integrated to establish the correct proportions of cells with particular fates is not known. We study this question in the context of the fate decision between embryonic epiblast (Epi) and extraembryonic primitive endoderm (PrE) that occurs in the mammalian preimplantation embryo. Using an embryonic stem cell system to model this decision in culture, we find that FGF/MAPK signaling determines the threshold concentration of GATA transcription factors required for PrE-like differentiation, and thereby controls the proportion of cells differentiating along this lineage. Our findings can be explained by a simple mutual repression circuit modulated by FGF/MAPK signaling. This may be a general network architecture to integrate the activity of signal transduction pathways and transcriptional regulators, and serve to balance proportions of cell fates in several contexts.

Introduction

To ensure the faithful development of multicellular organisms, cell fate decisions in populations of undifferentiated cells have to be tightly balanced. It is now well established that transcriptional networks and extracellular signals together control fate decisions, but how their interactions determine the proportions of cells adopting particular fates is not known. Classical genetic studies tend to emphasize hierarchical, linear relationships between these molecules, but in recent years it has become clear that rather than being linchpins in linear chains, the molecules involved in cell fate decisions form interconnected information processing networks. Understanding the mechanisms that balance fate decisions in populations requires insight into the dynamic activity these networks, and investigating how these dynamics are influenced by the network's components.

The first cell fate decisions in the mouse preimplantation blastocyst provide good models to study this question. After the first cleavages, blastomeres first commit to contributing either to the trophectoderm or the inner cell mass (ICM) lineages (Saiz and Plusa, 2013). Cells of the ICM then undergo a second decision to become epiblast (Epi) or extraembryonic primitive endoderm (PrE) (Rossant and Tam, 2009). The Epi lineage comprises the cells that will give rise to the embryo proper, whereas the PrE lineage forms the seed for extraembryonic tissues that function in patterning and nutrient supply of the developing embryo. Although the Epi and the PrE form separate tissues at the time of implantation, the decision to become either of them does not depend on the position of the cells in the embryo (Chazaud et al., 2006; Plusa et al., 2008).

Before ICM cells commit to the Epi or the PrE fate, they co-express transcriptional regulators for either lineage, such as the homeodomain protein Nanog, which is required for establishing the pluripotent Epiblast (Chambers et al., 2007; Silva et al., 2009), and the zinc-finger protein GATA6, which is essential to establish the PrE lineage (Bessonnard et al., 2014; Schrode et al., 2014). As embryos develop, cells acquire mutually exclusive expression of Nanog and GATA6, indicating acquisition of the Epi and PrE fate, respectively. The differentiation of GATA6-positive PrE cells requires an intact FGF/MAPK signaling pathway (Chazaud et al., 2006), and embryos mutant for the ligand FGF4 initially express GATA6, but fail to maintain its expression and to establish a mature PrE (Kang et al., 2012). Conversely, overactivation of FGF/MAPK signaling using recombinant ligand leads to the downregulation of Nanog in all cells and continued expression of GATA6 throughout the ICM (Kang et al., 2012; Yamanaka et al., 2010). These observations indicate that FGF/MAPK signaling is promotes PrE identity and inhibits Epi differentiation in ICM cells. In addition, the transcriptional regulators that mark the respective lineages play crucial roles in controlling fate choice in the ICM. Single ICM cells depleted for Nanog for example express the PrE markers GATA6, GATA4 and SOX17 at the late blastocyst stage (Frankenberg et al., 2011), and in Gata6 mutant embryos, all ICM cells continue to express Nanog (Bessonnard et al., 2014; Schrode et al., 2014). Based on these observations, it has been proposed that mutually repressive interactions between the Epi- and PrE-specific transcriptional programs amplify small random fluctuations in their initial activation in the early blastocyst, and thereby control lineage choice (Frankenberg et al., 2011; Schrode et al., 2014). How FGF/MAPK signaling impacts on these putative mutually repressive interactions, and how the

activities of transcriptional regulators and signaling are integrated to control the proportions of cells with alternative fates in the ICM is not known.

The factors guiding extraembryonic endoderm differentiation can be studied in embryonic stem (ES) cells, clonal derivatives of cells of the pre-implantation blastocyst, which display molecular and functional characteristics of the pluripotent epiblast. Under certain circumstances, these cells can populate extraembryonic lineages in chimeric embryos (Beddington and Robertson, 1989; Morgani et al., 2013), suggesting that they harbor a latent extraembryonic differentiation potential. Furthermore, ES cells can differentiate in culture into extraembryonic endoderm-like cells, either spontaneously over long time scales (Cho et al., 2012) or more rapidly upon forced expression of GATA4 or GATA6 (Fujikura et al., 2002; Shimosato et al., 2007). The spontaneous differentiation of ES cells into extraembryonic endoderm-like cells in culture is dependent on FGF/MAPK signaling (Cho et al., 2012), although forced transcription factor expression can bypass the requirement for some components of this signaling cascade (Wang et al., 2011).

Extraembryonic endoderm-like differentiation in ES cells thus recapitulates key requirements of PrE differentiation in the embryo. Here we use ES cells carrying inducible transgenes together with live reporters for the embryonic and extraembryonic fate to study, at the single cell level and with high temporal resolution, the interaction between FGF/MAPK signaling and GATA centered transcriptional networks in controlling the choice between embryonic and extraembryonic fates. By transient expression of GATA factors in ES cells we recreate a state of co-expression of Epi and PrE determinants akin to the state of ICM cells in the embryo. We find that stable PrE-like differentiation occurs from this state in cells exposed to GATA factor levels above a threshold dose, the magnitude of

which is set by the level of MAPK signaling. We recapitulate these experimental observations in a minimal model of mutual repression between the transcriptional networks underlying embryonic and extraembryonic fates, in which MAPK signaling inhibits the expression of the Epi-specific program. In both model and experiment, FGF/MAPK signaling acts as a rheostat to control the proportions of cells acquiring each of the alternative fates by modulating the behavior of transcriptional networks. This suggests a mechanism by which signaling balances the proportions of cells adopting specific fates, both in the ICM and beyond.

Results

An ES-cell model system to investigate PrE-like fate choice in culture

As ICM cells decide between epiblast and extraembryonic endoderm fates, they transition from a state of Nanog and GATA6 co-expression to one of mutually exclusive expression of Epi and PrE markers in individual cells (Plusa et al., 2008). To model the process of the resolution of this co-expression state in cultured cells, we transiently expressed a FLAG-tagged GATA6 transgene under the control of a doxycycline-inducible promoter (Beard et al., 2006) in ES cells (Fig. 1A). After 6h of doxycycline treatment, individual cells co-expressed inducible GATA6-FLAG and endogenous Nanog protein (Fig. 1B). 24h after a 6h doxycycline pulse, the exogenous GATA6-FLAG was completely degraded, but a subset of cells now stained positive for the endogenous PrE marker GATA4 in a pattern that was mutually exclusive with Nanog expression at the single cell level (Fig. 1C). We conclude that the transition from a GATA6/Nanog co-expression state to mutually exclusive expression of Epi- and PrE markers as it occurs in the ICM can be modeled in ES cells.

Previous studies have shown that GATA4 and GATA6 have equivalent capacity to induce PrE-like differentiation (Fujikura et al., 2002; Shimosato et al., 2007). We confirmed this using doxycycline-inducible expression of GATA4 and observed that this induced the same pattern of PrE-marker expression as inducible GATA6 expression, but in a larger proportion of cells (Fig. 1 D – F, Supplementary Figure S1). For this reason we decided to induce PrE-like differentiation with GATA4 and to use endogenous GATA6 expression to monitor the differentiation event. Furthermore, to follow the heterogeneous expression of the doxycycline-induced transgene in individual live cells, we expressed a GATA4-mCherry fusion protein under doxycycline control. This fusion protein retains biological activity to induce PrE-like

differentiation (Supplementary Figure S2), and was used in all subsequent experiments.

ES cell state affects the accessibility of the PrE-like differentiation program

For an induced transcription factor to trigger a specific differentiation program, this program needs to be molecularly accessible. ES cells have been shown to sample states with different potencies in a manner that depends on the culture medium (Macfarlan et al., 2012; Morgani et al., 2013), prompting us to explore the effects of exposing ES cells grown in different culture conditions to a pulse of GATA4-mCherry protein. In cells grown in the presence of feeders and 15% serum (the standard culture conditions used to derive inducible cell lines), transient GATA4-mCherry expression induced by a 6h pulse of doxycycline led to expression of endogenous GATA6 in approximately 10% of the cells the following day (Supplementary Figure S3A, B). In the absence of feeders and 10% serum, only approximately 1.5% of all cells were GATA6 positive 30h after a 6h doxycycline pulse, even though GATA4-mCherry was efficiently induced in this culture condition (Supplementary Figure S3C), and cells were positive for the pluripotency marker Nanog (Supplementary Figure S3A). Since culturing ES cells in 2i + LIF medium has been shown to promote extraembryonic potency (Morgani et al., 2013), we pre-cultured cells in 2i + LIF medium before simultaneous addition of doxycycline and transfer into serum-containing medium. This treatment regime increased the proportion of GATA6-positive cells induced by a 6h doxycycline pulse from 11.3 ± 1.8 % (mean ± standard deviation (SD)) for 1 day of pre-culture in 2i + LIF to 51.7 ± 9.8 % for 7 days of pre-culture (Fig. 2A - C). Because the efficiency of GATA4-mCherry expression following a 6h doxycycline pulse also changed with the

duration of the pre-culture in 2i + LIF (Supplementary Figure S4A), we determined the ratio between the fraction of GATA6-positive cells one day after a 6h doxycycline pulse and the fraction of GATA4-mCherry-positive cells immediately after the pulse as a measure for the efficiency of PrE-like differentiation. This ratio plateaus at approximately 0.55 after 3d of pre-culture in 2i + LIF (Fig. 2C), indicating that the accessibility of the PrE-like differentiation program can be restored in ES cell cultures by culture in 2i + LIF medium in a time-dependent manner.

To assess the influence of each of the components in 2i + LIF on the restoration of the PrE-like differentiation potential, we removed each of them from the complete 2i + LIF medium or added them individually to serum-containing medium during 3 days of pre-culture. All conditions led to an increase in the percentage of GATA6-positive cells 24h after a 6h doxycycline treatment, albeit to different degrees (Fig. 2D, E, F). The largest proportion of GATA6-positive cells was obtained for pre-culture in a medium containing serum, LIF and the Mek inhibitor PD0325901 (PD03), where the ratio between the fraction of GATA4-mCherry-positive cells 6h after the doxycycline pulse and the fraction of GATA6-positive cells one day later reached a value of 0.72 ± 0.02 (Fig. 2F, Supplementary Figure S4C). We conclude that inhibition of MAPK signaling prior to the induced expression of GATA factors efficiently restores extraembryonic differentiation potential in ES cell cultures. For all following experiments, we therefore pre-cultured cells for 3d in the presence of PD03 in medium containing serum and LIF. Importantly, this culture regime coupled to a 6h doxycycline pulse gives a proportion of ES cells undergoing PrE-like differentiation that is similar to the proportion of cells differentiating into PrE in the ICM of a mouse embryo (Schrode et al., 2014).

Transient expression of exogenous GATA4-mCherry induces stable PrE-like differentiation

Having established experimental conditions to induce PrE-like differentiation in ES cells with an efficiency mimicking PrE differentiation in the embryo, we wanted to investigate the stability of the GATA6-positive state and the dynamics with which it evolved. Measurement of endogenous GATA6 and Nanog expression in single cells by immunostaining one day after the doxycycline pulse showed that GATA6-positive cells stained negative for Nanog and vice versa (Fig. 3A), confirming that Nanog and GATA6 mark mutually exclusive states. To test whether these states were stable after removal of the transient GATA4-mCherry input, we created an H2B-Venus transcriptional reporter for Gata6 expression in cells carrying the inducible GATA4-mCherry transgene. Immunostaining and flow cytometry showed that cells with high expression levels of the reporter stained positive for endogenous GATA6 expression from the remaining endogenous allele one day after a 6h doxycycline pulse (Fig. 3B, C). This indicates that knock-in of the reporter does not affect PrE-like differentiation, and that it can be used to follow endogenous Gata6 expression. Between 32h and 80h after the end of the doxycycline pulse, the Venus expression profile in the population displayed a characteristic bimodal distribution, consisting of a $Venus^{negative}$ and a $Venus^{high}$ peak (Fig. 3D, E). The Venus expression levels of cells in the $Venus^{high}$ peak remained constant, but the number of cells in this peak slowly decreased over time (Fig. 3D, E). This was not due to a loss of Gata6 expression in individual cells, because $Venus^{high}$ cells sorted by flow cytometry did not revert to the $Venus^{negative}$ regime over a period of 48h (Fig. 3F). Transient GATA4-mCherry expression therefore induces stable expression of a marker for PrE-like differentiation.

To follow the dynamics of Gata6:H2B-Venus reporter expression over time in individual cells, we performed time-lapse microscopy of reporter cells permanently expressing the nuclear marker H2B-Cerulean to facilitate tracking of cells (Supplementary movie S1). H2B-Venus fluorescence intensity driven by the Gata6 promoter increased in individual cells approx. 8h after the start of the doxycycline pulse. Hierarchical clustering of traces according to H2B-Venus expression levels identified two distinct clusters containing cells with high and low Venus expression, respectively (Supplementary Figure S5, Fig. 3G). Expression levels of cells in each of the peaks were separated throughout the experiment, and we did not observe any cells that reverted from high expression levels back to low levels (Fig. 3G). Taken together, these results indicate that a transient GATA4-mCherry input elicits stable expression of one of two mutually exclusive expression programs. These are the hallmarks of a bistable switch.

A threshold level of GATA4-mCherry controls PrE differentiation

We then asked whether the turning of the bistable switch that we had identified depended on the expression levels of the doxycycline-induced GATA4-mCherry protein. We first tested different lengths of doxycycline exposure, which increased both the fraction of GATA4-mCherry positive cells and the maximum level of GATA4-mCherry expression in individual cells shortly after the end of the pulse (Supplementary Figure S6). Successively longer doxycycline pulses translated into an increase in the proportion of Gata6:H2B-Venus^{high} cells 24h after the end of the pulse (Fig. 4A, B), but H2B-Venus expression levels in individual cells were independent from doxycycline pulse length (Fig. 4A). This reaffirms the switch-like behavior of the differentiation event, because the expression level of the differentiated state does

not carry information about the strength of the transient input. Furthermore it suggests that GATA4-mCherry expression levels control the proportion of cells with PrE-like differentiation in the culture.

To further explore this idea, we sorted cells expressing GATA4-mCherry immediately after a doxycycline pulse into highly and lowly expressing fractions (Supplementary Figure S7). The proportion of differentiating GATA6-positive cells was higher following strong expression of GATA4-mCherry compared to low-level expression of the exogenous transcription factor (Fig. 4C, D). Furthermore, a large number of Nanog-positive undifferentiated cells were detected amongst the progeny of GATA4-Cherry^{low} cells (Fig. 4C), indicating that some low levels of GATA4-mCherry do not trigger PrE-like differentiation. To measure GATA4-mCherry input levels in single cells more precisely and relate them to subsequent fate choice, we performed time-lapse imaging of GATA4-mCherry-inducible cells expressing a H2B-Cerulean marker during and after a doxycycline pulse, followed by immunostaining for Nanog and GATA6 (Supplementary Movie S2 and Supplementary Figure S8A, B). This revealed that the average mCherry expression levels in cells that gave rise to GATA6-positive progeny (purple in Fig. 4E,F, Supplementary Figure S8C) were higher than in those cells whose progeny was Nanog-positive (green datapoints in Fig. 4E, F, Supplementary Figure S8C). Because there was only little overlap between the two classes of traces, we tested how well fate choice could be predicted from GATA4-mCherry expression levels with a threshold-based classifier and analyzing its performance in receiver operating characteristics (ROC) (Fawcett, 2006). In this analysis, a threshold level of GATA4-mCherry expression is used to make a prediction based on the assumption that all cells above the threshold will differentiate, and those below it will not. This prediction is then compared to the real outcome, and

for each threshold level the ratio of correct and false predictions to the overall number of events is determined (true positive ratio TPR, and false positive ratio, FPR). Plotting FPR versus TPR for all threshold values gives a characteristic curve (Fig. 4G), and the area under this curve (AUC) is a measure of the ability of a classifier to predict an outcome – classifiers without predictive value have an AUC of 0.5, while a perfect predictor gives an AUC of 1.0. For our dataset, the AUC increased quickly upon doxycycline addition and reached a plateau between 0.8 and 0.9 approx. 3 h after doxycycline addition (Fig. 4H), indicating that GATA4-mCherry expression levels are a good predictor for final fate outcome soon after induction of its expression. In each timepoint, we also calculated the optimal threshold for the prediction of fate choice, which we defined as the threshold that maximizes the difference between the true and false positive prediction rates (red point in Fig. 4G). This optimal threshold tracked the expression dynamics of the GATA4-mCherry protein (black line in Figure 4E), and separated most fluorescence intensity tracks of cells with Nanog-positive progeny from those that gave GATA6-positive progeny (black line in Figure 4F, Supplementary Figure S9A, B). Using this threshold, the accuracy of fate prediction based on GATA4-mCherry expression levels reached values above 0.8, i.e. 80% of all fate decisions could be correctly predicted based on the GATA4-mCherry classifier (Supplementary Figure S9C). These results suggest that in the ES cell system, fate choice can be largely predicted from GATA4-mCherry levels, and is likely determined by the activity of this transcription factor.

FGF/MAPK modulates the probability of PrE-like fate choice

In the mouse embryo, both GATA factors and FGF/MAPK signaling are required to establish PrE identity. Having shown above that inhibition of MAPK signaling is

required to make the extraembryonic differentiation program accessible in ES cells, we wanted to test how the levels of MAPK signaling affected the decision to embark on PrE-like differentiation following induced GATA expression. The peak levels of Erk phosphorylation resulting from removal of full Mek inhibition by 1 μM PD03 in the pre-culture medium (Supplementary Fig. S10) could be smoothly tuned by transferring cells to subsaturating concentrations of PD03 (Fig. 5A). Partial inhibition of signaling using these subsaturating PD03 concentrations during the 6h doxycycline pulse and the 24h chase period reduced the fraction of GATA6 positive cells, but not the expression levels of GATA6 in individual differentiated cells (Fig. 5B, C). We found a quasi-linear relationship between the level of Erk phosphorylation and the percentage of differentiating cells (Fig. 5D), indicating that MAPK signaling levels control the fraction of cells that embark on the PrE-like differentiation path. To investigate how partial Mek inhibition by PD03 affected the GATA4-mCherry expression levels required for extraembryonic differentiation, we performed time-lapse imaging and cell tracking for maximal and reduced MAPK signaling in parallel. In the presence of 62.5 nM PD03, a concentration led to a significant reduction of the number of differentiating cells but gave enough GATA6 positive cells for statistical analysis (Fig. 5C), cells with GATA6-positive progeny had expressed higher GATA4-mCherry levels than cells whose progeny was Nanog-positive, similar to the situation without signaling inhibition (Fig. 5E, F). However, the distribution of GATA4-mCherry expression levels in the two classes changed upon partial inhibition of signaling: While in the absence of PD03, virtually all GATA4-mCherry^{high} cells differentiated, upon partial Mek inhibition GATA4-mCherry^{high} cells had both differentiated and undifferentiated progeny. Conversely, GATA4-mCherry^{low} cells almost never differentiated in the presence of 62.5 nM PD03, while in the absence of

PD03 GATA4-mCherry^{low} cells gave rise to both differentiated and undifferentiated progeny (Fig. 5F). Despite these changed distributions, differentiation could still be predicted based on GATA4-mCherry expression levels, as the AUC in the presence of 62.5 nM PD03 reached a maximum value of 0.8 approx. 3h into the experiment, similar to the condition without Mek inhibition (Fig. 5G). Importantly, when we compared the optimal threshold for the prediction of differentiation based on GATA4-mCherry expression levels for different signaling regimes, we found that this was consistently increased upon partial Mek inhibition (Fig. 5F, H). Taken together, this indicates that MAPK signaling levels control the fraction of differentiating cells for a given range of transcription factor input by setting the GATA4-mCherry threshold level required to trigger differentiation.

A simple mutual repression circuit recapitulates the experimentally observed gene expression dynamics

Having shown that MAPK signaling sets the threshold of GATA4-mCherry required for PrE-like differentiation, we decided to use our measurements to create a minimal model of the decision event in order to gain insights into the formal nature of the interactions between the levels of GATA and MAPK signaling. The observation that the differentiation event displayed hallmarks of bistability (Figure 3) led us to start with a network of two mutually repressive nodes, Gata (*G*) and Nanog (*N*), the simplest system that gives this type of dynamic behavior (Plahte et al., 1995; Snoussi, 1998; Thomas, 1981) (Fig. 6A, see Materials and Methods for a detailed description of the model). The model accounts for the behavior of individual cells, which are assumed to initially express high levels of Nanog and no GATA to reflect pre-culturing in the presence of PD03. We modeled the dynamics of Nanog, endogenous

GATA and the externally supplied pulse of GATA (G_X) in single cells with ordinary differential equations. The only source of cell-to-cell heterogeneity in our model was the maximum transcription rate of exogenous GATA, to reflect the experimentally observed heterogeneous expression of exogenous GATA factors from the doxycycline-inducible promoter.

The general dynamics of the endogenous circuit described by this model can be assessed in the GATA-Nanog phase space (Fig. 6B). For the specific set of parameter values used here, the nullclines ($dG/dt=0$ $dN/dt=0$) cross thrice, generating three equilibrium states, two of which are stable and correspond to the fully differentiated GATA-positive and the undifferentiated Nanog-positive state, respectively (Fig. 6B). Combinations of Nanog and GATA levels outside these stable points will change over time and converge to one of the stable points, depending on where in the phase space a given combination of Nanog and GATA levels is located. To induce PrE-like differentiation, the exogenous GATA input has to be to strong enough to allow for sufficient Nanog repression and endogenous GATA expression to move a cell across the boundary (dashed line in Fig. 6B) that separates the combinations of GATA and Nanog levels leading to the fully differentiated GATA-positive from those that lead to the undifferentiated Nanog-positive state. This boundary in the phase space translates into a threshold for exogenous GATA levels that perfectly separates the cells according to the fate that they will eventually adopt. For the chosen parameter set, simulated time traces of individual cells closely resembled the experimentally observed expression dynamics of endogenous GATA G (Fig. 6C, compare to Fig. 3G), and exogenous GATA4-mCherry G_X (Fig. 6D, compare to Fig. 4E), suggesting this simple mutual repression circuit is sufficient to capture essential dynamics of the experimental system.

To further test the model, we compared the dynamics of Nanog expression *in silico* and *in vivo*. In model simulations, Nanog expression levels initially decreased rapidly in all cells from the initial conditions chosen to represent the effects of the pre-culture regime towards much lower steady state levels. Only at a later stage of the simulation, differences in the Nanog expression levels between cells that activate endogenous GATA *G* and those that do not became apparent (Fig. 6E). To measure endogenous Nanog levels experimentally, we knocked a translational Nanog fusion reporter (Filipczyk et al., 2013) into the inducible GATA4-mCherry cell line and performed time-lapse imaging during and after a doxycycline pulse, followed by immunostaining for fate markers. Expression of the Nanog-Venus reporter initially decreased in all cells following removal of the pre-culture medium (Supplementary Movie S3, Fig. 6F). Approx. 10h after removal of PD03 and addition of doxycycline, we detected small differences between those cells that eventually stained GATA6-positive and those were Nanog-positive at the end of the experiment (Supplementary Movie S3, Fig. 6F). This agreement between Nanog expression dynamics *in silico* and *in vivo* further supports the idea that a simple mutual repression circuit is sufficient to capture the dynamics of the system.

Inhibition of the Epi program by MAPK signaling controls the proportion of cells with PrE-like differentiation

We then wanted to pinpoint the main mechanism by which FGF/MAPK signaling controls the fraction of cells with PrE-like differentiation, using our mathematical model as a guide. We considered two simple extensions of the model, one in which FGF/MAPK signaling inhibits the Epi program centered on Nanog (Fig. 7A), and an alternative model in which signaling promoted expression of the PrE program

characterized by GATA (Fig. 7B). We ran simulations for different signaling levels for both model architectures (for details see Materials and Methods) and assessed the fractions of Nanog- and GATA-positive cells, as well as the protein expression levels within these populations. Both model architectures gave bimodal distributions for GATA- and Nanog expression, and in either case a reduction of signaling led to an increase in the number of cells in the Nanog-high peak and a decrease of cells in the GATA-high peak (Fig. 7 A, B, middle panels). However, if signaling was assumed to activate Gata expression, GATA levels in the GATA-positive peak decreased at lower signaling, whereas Nanog expression levels were independent of signaling levels (Fig. 7A, middle panels). In the alternative architecture, Nanog expression levels increased at lower signaling levels, while GATA levels were independent of signaling (Fig. 7B, middle panels). To distinguish experimentally how FGF/MAPK signaling controlled the mutual repression circuit, we measured GATA6 and Nanog expression levels in the respective positive populations at different signaling regimes. We used Nanog-Venus reporter cells and stained them with an antibody detecting the Venus fluorescent protein to determine Nanog expression levels in the Nanog-positive population, because this method detected a bimodal distribution of Nanog-Venus-positive and –negative cells with a higher signal-to-noise ratio than direct staining for Nanog (Fig. 7C). From flow cytometry data of these cells, and cells that had been stained for GATA6 expression, we determined peak positions (Supplementary Figure S11), and calculated the fold-change between the position of the positive and the negative peak to correct for different staining efficiencies between samples. This analysis did not detect a consistent trend in changes of GATA6 expression levels with increasing doses of PD03, i.e. its levels remained approximately constant, while the Nanog-Venus positive peak consistently shifted to higher expression levels with

lowered signaling (Fig. 7D). While not ruling out a more complex integration of FGF/MAPK signaling into the regulatory circuit that we have described, these results suggest that the main route by which FGF/MAPK signaling controls the fraction of cells with PrE-like differentiation is through inhibition of the Epi-specific gene expression program.

To develop an intuitive, visual representation of the system's dynamics in different signaling regimes, we estimated the path-integral quasi-potential surfaces (Bhattacharya et al., 2011) of our system for two different signaling levels (Fig. 7 E, F). This landscape representation, in which cells can be depicted to roll towards lower potential levels, highlights two basins of attraction corresponding to the Nanog-positive state and the GATA positive state, respectively. A reduction in signaling shifts the Nanog-positive basin towards higher Nanog levels and bends the ridge that separates the basins towards the GATA-positive state, thereby making its basin of attraction narrower and shallower relative to that of the Nanog-positive state (Fig. 7 E, F).

In summary we conclude that a simple mutual repression circuit controls the decision between the Epi and the PrE fate modeled in culture, and that the main input of FGF/MAPK signaling into this circuit occurs through repression of the Epi program. This allows signaling to regulate the proportions of cells adopting either fate by setting the relative sizes of the basins of attraction corresponding to the two states.

Discussion

We have used mouse ES cells to model the decision between the Epi and the PrE fate that occurs in ICM cells of the developing embryo. Our *in vitro* experimental system allows us to modulate and measure the transcription factor and signaling inputs into the decision quantitatively, and live cell reporters for Nanog and Gata6 expression enable us to follow the dynamics of the decision at the level of single cells. The ES cell system recapitulates the gene expression dynamics of key marker genes of the decision in the embryo, suggesting that the underlying mechanism of the fate decision is the same in both settings. We have uncovered two successive functions of MAPK signaling in the ES cell system: Before the induced expression of GATA factors, inhibition of MAPK signaling is required to make the extraembryonic differentiation program accessible to ES cells. Once exogenous GATA factors are expressed, MAPK signaling is required to execute the decision of PrE-like differentiation. This differentiation event displays hallmarks of an irreversible bistable switch, as co-expression of markers of the embryonic and extraembryonic fates resolves into one of two mutually exclusive stable states characterized by Nanog and GATA expression, respectively. We detect a threshold level of exogenous GATA factor expression required to turn this switch and induce differentiation, and find that MAPK signaling sets this threshold dose. The decision to differentiate is therefore a strongly regulated irreversible process, largely determined by the combination of transcriptional and signaling activity in individual cells.

The accessibility of the PrE program depends on ES cell state

In the embryo, the decision of a cell to become Epi or PrE can be separated into two phases. In a first step, cells in the embryo make both differentiation programs

molecularly available, as reflected in the co-expression of transcriptional regulators for the two fates. In a second step, individual cells choose and implement one of the two fates, and make the alternative inaccessible. We find that in ES cells, the accessibility of the PrE-like differentiation program from this co-expression state is a function of previous culture conditions: Cells cultured in the presence of serum are refractory to PrE-like differentiation, but this program can be made readily available by extended exposure to GSK3 or Mek inhibitors, e.g. in 2i medium. One interpretation of this finding is that ES cells cultured in serum are strongly biased towards embryonic fates, and as a consequence have blocked the extraembryonic endoderm differentiation program. In line with this idea, a recent study comparing the transcriptomes of ES cells and ICM cells suggests that ES cells cultured in 2i medium resemble an earlier developmental state than cells cultured in serum + LIF (Boroviak et al., 2014). It has been shown that individual ES cells can sample accessibility to a range of early differentiation programs over time (Macfarlan et al., 2012; Morgani et al., 2013), and the presence of GSK3 and Mek inhibitors may favour a more naïve ES cell state that has the PrE-like differentiation program accessible and mirrors the situation of early ICM cells. A genome-wide study of chromatin marks revealed that ES cells grown in the presence of serum display higher levels of repressive chromatin marks on a subset of promoters, including the Gata6 promoter, than cells grown in 2i + LIF (Marks et al., 2012), and these repressive chromatin marks may block PrE-like differentiation. Our finding that few cells with high exogenous GATA4-mCherry expression do not embark on PrE-like differentiation even from culture conditions that make the differentiation program accessible in most cells may reflect persistent heterogeneous chromatin configurations in cells in the population. Alternatively, the inability to respond to induced GATA expression may be a consequence of

heterogeneous MAPK signaling amongst ES cells, which has been detected in other cell lines (Albeck et al., 2013; Aoki et al., 2013), and which we expect will be functionally relevant for PrE-like differentiation of ES cells. That the response to forced transcription factor expression depends on a cells' state has been known for a long time (Cahan et al., 2014; Weintraub et al., 1989); the dynamic changes in the accessibility of the extraembryonic differentiation program in ES cells may become a fruitful model to further explore the underlying molecular mechanisms of this phenomenon.

Extraembryonic fate choice is determined by the output of a simple mutual repression circuit

We have shown here that precise measurements of GATA4-mCherry expression levels allow prediction of fate decisions in individual ES cells with high confidence before endogenous fate markers appear, which led us to formalize the underlying mechanism in a minimal model of the underlying genetic circuit. This mathematical model consists of mutually repressive interactions between the Epi program, centered on Nanog, and the extraembryonic endoderm program, centered on GATA factors, modulated by a repressive input of FGF/MAPK on the Epi program (Fig. 6A, G). The model assumes deterministic regulation and yet fits remarkably well with key experimental observations, such as bistability at the level of single cells, dependence of the fraction of differentiating cells on both transcription factor and signaling levels, and, finally, the dynamics of expression of the markers for the differentiated PrE-like and the undifferentiated Epi-like state. In particular, the model mirrors the experimental finding that the role of MAPK signaling is to set a GATA threshold required for the extraembryonic endoderm fate to be implemented: whether a cell will

differentiate depends on the combination of GATA and MAPK activity. This network model therefore replaces the epistatic, linear views of the relationships between signal transduction pathways and transcriptional networks with a picture wherein both inputs are quantitatively integrated to arrive at a fate decision.

The minimal model that we identify here is a subnetwork of a more complex model of this fate decision recently proposed by Bessonard et al. (2014). Bessonard's model posits an additional positive input of FGF/MAPK signaling onto Gata expression, and contains positive autoregulatory feedback loops centered on both Nanog and Gata, which endow the dynamic system with a third stable state of Nanog and GATA co-expression. This allowed Bessonard et al. to simulate both the establishment and the resolution of the co-expression state in a single model. Our approach focuses on the resolution of the co-expression state, and comparison of gene expression dynamics with the simulation results of the minimal model suggests that the additional links of Bessonard's model are not required to explain the dynamics of this phase of the decision. It remains however possible that positive autoregulation of the Epi and PrE programs and a positive input of FGF/MAPK signaling on Gata expression fine-tune the response of cells during this second stage of the lineage decision process.

Integration of signaling into the mutual repression circuit serves to balance proportions of cell fates in developing tissues

The mathematical model of a mutual repression circuit has previously been applied to describe the dynamics of the switch between the lysogenic and lytic phases of the lifecycle of bacteriophage lambda (Ptashne, 2004), and a genetically engineered toggle switch circuit in E. coli (Gardner et al., 2000). Our work is one of the first to suggest that this network can be used to formalize the decision between two fates

during mammalian development. Furthermore, we show that extending this model with a signaling input allows for dynamic control of the sizes of the basins of attraction corresponding to the different states of the bistable system. The mammalian preimplantation embryo may harness this property to balance the proportion of Epi and PrE cells. The initial expression of transcriptional regulators driving lineage choice appears to be stochastic due to the mechanisms that control gene expression in the early embryo (Dietrich and Hiiragi, 2007; Ohnishi et al., 2014), and the resulting heterogeneous distribution of transcription factor concentrations in ICM cells will bias cells towards specific fates. It has been shown that lineage commitment occurs non-synchronously in the cells of the ICM, and that the first cells to commit are fated towards the epiblast (Grabarek et al., 2012). Because Epi cells produce FGF4 (Frankenberg et al., 2011; Nichols et al., 1998), the extent of FGF4 production will therefore be a function of the number of Epi-committed cells and act on the as-yet uncommitted cells. By modulating the bistable switch operating in these cells, this process may ultimately place the appropriate number of uncommitted in the basin corresponding to the PrE fate. FGF/MAPK signaling might thus acts as feedback mechanism to balance proportions of two distinct cell fates in populations. It will be interesting to see whether this new principle applies to differentiation decisions beyond those in the preimplantation embryo.

Materials and Methods

ES cell culture and genetic manipulation

For derivation of genetically modified lines, ES cells were grown on mitotically inactivated mouse embryonic fibroblasts in Knockout DMEM (Gibco) supplemented with 15% fetal bovine serum, 50µM beta-mercaptoethanol, glutamax, non-essential amino acids and leukemia inhibitory factor (LIF, Department of Biochemistry, University of Cambridge). After line derivation, feeders were removed by serial passaging, and cells were maintained on gelatin coated dishes in GMEM-based medium supplemented with 10% fetal bovine serum, sodium pyruvate, 50µM beta-mercaptoethanol, glutamax, non-essential amino acids and leukemia inhibitory factor. All cell lines used in this study were based on the KH2 ES cell line described in Beard et al., 2006, and inducible cell lines were generated as described (Beard et al., 2006). Transgene induction was induced by adding 500 ng/ml doxycycline to the culture medium. The Gata6 reporter cell line was generated using knock-out first targeting arms of the EUCOMM project (Skarnes et al., 2011), combined with a H2B-Venus reporter cassette and a neomycin resistance gene driven from a human β-actin promoter. The targeting construct to generate the Nanog-Venus translational fusion has been described previously (Filipczyk et al., 2013). The construct used for permanent expression of the H2B-Cerulean marker was generated from pCX::H2B-mCherry described in (Nowotschin et al., 2009) by replacing the mCherry coding sequence with a Cerulean coding sequence. To generate reporter lines, approx. $2*10^6$ cells were electroporated with 2 µg of the linearized targeting vector, plated onto feeder cells and put under selection one day after electroporation. Resistant colonies were picked after seven days, and PCR genotyped for correct insertion events. Karyotypes of all genetically modified clones were determined according to standard

procedures (Nagy et al., 2008), and clones with a median chromosome count of 40 were selected for experiments. Two subclones of the cell line carrying the inducible Gata4-mCherry construct were tested in blastocyst injections, and both gave high-contribution chimaeras with germline transmission.

Immunocytochemistry

Cells for immunocytochemistry were grown on ibidi μ-slides and stained according to standard procedures. Briefly, cells were washed once in PBS and fixed for 15 minutes in 4% PFA. Blocking and antibody incubation was performed in BBS/1%BSA/0.1%Triton. Primary antibodies used were anti-Nanog (eBiosciences, 1:200), anti-FLAG (Sigma M2, 1:1000), anti-GATA6 (R&D, 1:200) and anti-GATA4 (Santa Cruz, 1:200). Detection was performed using Alexa-Fluor conjugated secondary antibodies (Molecular Probes) at 1:500 dilution. Nuclei were visualized using Hoechst 33342 dye (Molecular Probes). Imaging was performed on a Zeiss LSM700 confocal microscope with a 40x oil immersion lens (NA 1.2). To quantify immunofluorescence intensity in single cells, images were segmented based on nuclear fluorescence using methods available in FIJI (Schindelin et al., 2012), and mean fluorescence intensities for individual channels measured in segmented regions after manual curation.

Flow cytometry

Cells for flow cytometry were trypsinized and either analyzed immediately or fixed for 15 minutes in 3% PFA/PBS. Staining of intracellular antigens was performed by blocking cells for at least 30 minutes in PBS/0.25%saponin/1%BSA and incubating with primary antibody overnight. Primary and secondary antibodies and dilutions

were the same as for immunostaining procedures. mCherry fluorescence was measured on a BectonDickinson Fortessa Flow cytometer, all other flow cytometric analysis was performed using a Beckman Coulter CyAn ADP analyzer. Cell sorting was done on a Beckman Coulter MoFlo. To estimate peak positions, histograms were smoothened, followed by detection of local maxima with custom-written Python scripts.

Immunoblotting

For immunoblotting, cells were lysed in RIPA buffer and lysates were separated on custom-made polyacrylamide gels before transfer to nitrocellulose membranes. Antibodies used were anti-ppErk (Sigma M9692) and anti-Erk1/2 (Millipore 06-182) at 1:500 dilution. Detection was performed using fluorescently labeled secondary antibodies and scanning in a LI-COR Odyssey system. Intensities of bands were quantified in ImageStudio (LI-COR).

Time-lapse imaging and cell tracking

Cells for time-lapse imaging were seeded at a density of approx. $1*10^4$ cells/cm^2 one day prior to imaging. Imaging was performed in DMEM based medium without phenol red, supplemented with 10% fetal bovine serum, sodium pyruvate, 50µM beta-mercaptoethanol, glutamax, non-essential amino acids and leukemia inhibitory factor. We used a Zeiss Axiovert M200 microscope equipped with a SOLA LED light source, an Andor iXON Ultra 888 EMCCD camera and a heated stage with CO_2 supply. Hardware was controlled by MicroManager software (Edelstein et al., 2001). Time-lapse movies were acquired using a 40x long-working distance lens and standard brightfield optics. Spatial heterogeneities in fluorescence intensity stemming

from uneven illumination across the field of view were removed by taking 50 flatfield images without any cells, and normalizing fluorescence intensities from experimental movies with the average of the flatfield images. Temporal heterogeneities in fluorescence signal in the movies due to varying illumination intensities and medium autofluorescence were removed by measuring fluorescence intensity for at least cell-free three positions per movie, and subtracting their average fluorescence values from all measured pixel intensities. For some experiments, cells were fixed and immunostained for marker gene expression and returned to the microscope for imaging. Cells were tracked manually using the MTrackJ plugin of ImageJ (Erik Meijering, 2012), and fluorescence intensities in a region of interest around the trackpoint were extracted with custom-written Python scripts.

Mathematical modeling

The mathematical model proposed is based on the well studied mutual repression circuit (Gardner et al., 2000) and describes the dynamics of Gata (G), Nanog (N), as well as externally induced Gata expression (G_X) (Figure 6 A) with the three following rate equations:.

$$\frac{dN}{dt} = \frac{\alpha_N}{1+(G+G_X)^p} - \lambda_N N$$
$$\frac{dG}{dt} = \frac{\alpha_G}{1+(N)^q} - \lambda_G G$$
$$\frac{dG_X}{dt} = D\pi_\tau(t) - \lambda_G G_X \quad .$$

The transient exogenous Gata G_X transcription rate was modeled with a rectangular step function π_τ of duration τ=6h. To account for the experimentally observed heterogeneity in the response to doxycycline, the maximum transcription rate parameter of G_X, D, was varied from cell to cell according to a log-normal distribution

with scale parameter σ_D. Gata and Nanog mutually repress each other's expression and this was accounted for by inhibitory Hill functions with cooperativity coefficients p and q. Exogenous Gata also participates in the repression of Nanog. For a given level of signaling, the maximal Gata and Nanog production rates α_G and α_N, which are attained in absence of their respective repressor, were assumed constant. Regarding the interaction of signaling with this transcription network, we have considered two scenarios. In the first one we assumed that the maximum transcription rate for Nanog decreases linearly with the signal level s, $a_N(s) = a_{N1}\, s + a_{N0}\,(1\text{-}s)$, where $a_{N1} \leq a_{N0}$ while the maximum Gata transcription rate is not affected. The second scenario we considered is a linear increase of the maximum Gata transcription rate with signal level, $a_G(s) = a_{G1}\, s + a_{G0}\,(1\text{-}s)$, $a_{G0} \leq a_{G1}$, and a constant Nanog transcription rate. In both cases signaling was assumed to be constant and equal in all cells. The model expresses concentrations normalized to the half-maximum inhibition concentration of the Hill functions, i.e., in arbitrary adimensional units. Time is expressed in dimensional units, and all protein decay rate values (λ_G and λ_N) were set to match the experimentally observed half lives (4-5 hours). Thus, all but four parameter values of this system were constrained by experimental data (see Supplementary table S1 for all parameters used for simulations). To reflect the pre-culturing of cells in the presence of PD03 we chose as initial condition for Nanog expression levels its steady state levels in the absence of signaling. Initial endogenous GATA levels were set to zero, reflecting the absence of detectable GATA expression in our ES cells in the absence of doxycycline stimulation. The visual representations of the potential landscape in Fig. 7E, F correspond to the path-integral quasi-potential surfaces as proposed by (Bhattacharya et al., 2011). These have been computed assuming no external supply of GATA factors. Parameter values used in the simulations are given in

Supplementary Table S1. Numerical simulations were implemented in Python language.

Acknowledgements

We thank K. Niakan for providing reagents that helped starting this project and K. Anastassiadis, B. Rosen, K. Lindon and A.-K. Hadjantonakis for sharing reporter constructs. L. Filipkova, N. S. Ly and R. Broome provided technical assistance, and L. Garcia-Perez, C. Vintiner and J. Padua helped with cell tracking. We are grateful to J. Nichols and A.-K. Hadjantonakis for insightful discussions, and C. Pina, J. de Navascués, S. Muñoz-Descalzo and C. Brimson for helpful comments on earlier versions of this manuscript. Work in the Martinez Arias lab was funded by an HFSP grant and an ERC investigator grant. CS was the recipient of an EMBO long-term fellowship, and CS and PR were supported by a Marie Curie fellowship from the European Union.

Conflict of Interest

The authors declare no conflict of interest.

References

Albeck, J.G., Mills, G.B., and Brugge, J.S. (2013). Frequency-modulated pulses of ERK activity transmit quantitative proliferation signals. Molecular Cell *49*, 249–261.

Aoki, K., Kumagai, Y., Sakurai, A., Komatsu, N., Fujita, Y., Shionyu, C., and Matsuda, M. (2013). Stochastic ERK activation induced by noise and cell-to-cell propagation regulates cell density-dependent proliferation. Molecular Cell *52*, 529–540.

Beard, C., Hochedlinger, K., Plath, K., Wutz, A., and Jaenisch, R. (2006). Efficient method to generate single-copy transgenic mice by site-specific integration in embryonic stem cells. Genesis *44*, 23–28.

Beddington, R.S., and Robertson, E.J. (1989). An assessment of the developmental potential of embryonic stem cells in the midgestation mouse embryo. Development *105*, 733–737.

Bessonnard, S., De Mot, L., Gonze, D., Barriol, M., Dennis, C., Goldbeter, A., Dupont, G., and Chazaud, C. (2014). Gata6, Nanog and Erk signaling control cell fate in the inner cell mass through a tristable regulatory network. Development *141*, 3637–3648.

Bhattacharya, S., Zhang, Q., and Andersen, M.E. (2011). A deterministic map of Waddington's epigenetic landscape for cell fate specification. BMC Syst Biol *5*, 85.

Boroviak, T., Loos, R., Bertone, P., Smith, A., and Nichols, J. (2014). The ability of inner-cell-mass cells to self-renew as embryonic stem cells is acquired following epiblast specification. Nature Cell Biology *16*, 516–528.

Cahan, P., Li, H., Morris, S.A., da Rocha, E.L., Daley, G.Q., and Collins, J.J. (2014). CellNet: Network Biology Applied to Stem Cell Engineering. Cell *158*, 903–915.

Chambers, I., Silva, J., Colby, D., Nichols, J., Nijmeijer, B., Robertson, M., Vrana, J., Jones, K., Grotewold, L., and Smith, A. (2007). Nanog safeguards pluripotency and mediates germline development. Nature *450*, 1230–1234.

Chazaud, C., Yamanaka, Y., Pawson, T., and Rossant, J. (2006). Early lineage segregation between epiblast and primitive endoderm in mouse blastocysts through the Grb2-MAPK pathway. Dev Cell *10*, 615–624.

Cho, L.T.Y., Wamaitha, S.E., Tsai, I.J., Artus, J., Sherwood, R.I., Pedersen, R.A., Hadjantonakis, A.-K., and Niakan, K.K. (2012). Conversion from mouse embryonic to extra-embryonic endoderm stem cells reveals distinct differentiation capacities of pluripotent stem cell states. Development *139*, 2866–2877.

Dietrich, J.-E., and Hiiragi, T. (2007). Stochastic patterning in the mouse pre-implantation embryo. Development *134*, 4219–4231.

Edelstein, A., Amodaj, N., Hoover, K., Vale, R., and Stuurman, N. (2001). Computer Control of Microscopes Using µManager (Hoboken, NJ, USA: John Wiley & Sons,

Inc.).

Erik Meijering, O.D.I.S. (2012). Methods for Cell and Particle Tracking. 1–16.

Fawcett, T. (2006). An introduction to ROC analysis. Pattern Recognition Letters *27*, 861–874.

Filipczyk, A., Gkatzis, K., Fu, J., Hoppe, P.S., Lickert, H., Anastassiadis, K., and Schroeder, T. (2013). Biallelic expression of nanog protein in mouse embryonic stem cells. Cell Stem Cell *13*, 12–13.

Frankenberg, S., Gerbe, F., Bessonnard, S., Belville, C., Pouchin, P., Bardot, O., and Chazaud, C. (2011). Primitive endoderm differentiates via a three-step mechanism involving Nanog and RTK signaling. Dev Cell *21*, 1005–1013.

Fujikura, J., Yamato, E., Yonemura, S., Hosoda, K., Masui, S., Nakao, K., Miyazaki Ji, J.-I., and Niwa, H. (2002). Differentiation of embryonic stem cells is induced by GATA factors. Genes Dev *16*, 784–789.

Gardner, T.S., Cantor, C.R., and Collins, J.J. (2000). Construction of a genetic toggle switch in Escherichia coli. Nature *403*, 339–342.

Grabarek, J.B., Zyzynska, K., Saiz, N., Piliszek, A., Frankenberg, S., Nichols, J., Hadjantonakis, A.-K., and Plusa, B. (2012). Differential plasticity of epiblast and primitive endoderm precursors within the ICM of the early mouse embryo. Development *139*, 129–139.

Kang, M., Piliszek, A., Artus, J., and Hadjantonakis, A.K. (2012). FGF4 is required for lineage restriction and salt-and-pepper distribution of primitive endoderm factors but not their initial expression in the mouse. Development *140*, 267–279.

Macfarlan, T.S., Gifford, W.D., Driscoll, S., Lettieri, K., Rowe, H.M., Bonanomi, D., Firth, A., Singer, O., Trono, D., and Pfaff, S.L. (2012). Embryonic stem cell potency fluctuates with endogenous retrovirus activity. Nature *487*, 57–63.

Marks, H., Kalkan, T., Menafra, R., Denissov, S., Jones, K., Hofemeister, H., Nichols, J., Kranz, A., Stewart, A.F., Smith, A., et al. (2012). The transcriptional and epigenomic foundations of ground state pluripotency. Cell *149*, 590–604.

Morgani, S.M., Canham, M.A., Nichols, J., Sharov, A.A., Migueles, R.P., Ko, M.S.H., and Brickman, J.M. (2013). Totipotent Embryonic Stem Cells Arise in Ground-State Culture Conditions. CellReports *3*, 1945–1957.

Nagy, A., Gertsenstein, M., Vintersten, K., and Behringer, R. (2008). Karyotyping Mouse Cells. Cold Spring Harbor ….

Nichols, J., Zevnik, B., Anastassiadis, K., Niwa, H., Klewe-Nebenius, D., Chambers, I., Schöler, H., and Smith, A. (1998). Formation of pluripotent stem cells in the mammalian embryo depends on the POU transcription factor Oct4. Cell *95*, 379–391.

Nowotschin, S., Eakin, G.S., and Hadjantonakis, A.-K. (2009). Dual transgene strategy for live visualization of chromatin and plasma membrane dynamics in murine

embryonic stem cells and embryonic tissues. Genesis *47*, 330–336.

Ohnishi, Y., Huber, W., Tsumura, A., Kang, M., Xenopoulos, P., Kurimoto, K., Oleś, A.K., Araúzo-Bravo, M.J., Saitou, M., Hadjantonakis, A.-K., et al. (2014). Cell-to-cell expression variability followed by signal reinforcement progressively segregates early mouse lineages. Nature Cell Biology *16*, 27–37.

Plahte, E., Mestl, T., and Omholt, S.W. (1995). Feedback Loops, Stability and Multistationarity in Dynamical Systems. J. Biol. Syst. *03*, 409–413.

Plusa, B., Piliszek, A., Frankenberg, S., Artus, J., and Hadjantonakis, A.-K. (2008). Distinct sequential cell behaviours direct primitive endoderm formation in the mouse blastocyst. Development *135*, 3081–3091.

Ptashne, M. (2004). A Genetic Switch (CSHL Press).

Rossant, J., and Tam, P.P.L. (2009). Blastocyst lineage formation, early embryonic asymmetries and axis patterning in the mouse. Development *136*, 701–713.

Saiz, N., and Plusa, B. (2013). Early cell fate decisions in the mouse embryo. Reproduction *145*, R65–R80.

Schindelin, J., Arganda-Carreras, I., Frise, E., Kaynig, V., Longair, M., Pietzsch, T., Preibisch, S., Rueden, C., Saalfeld, S., Schmid, B., et al. (2012). Fiji: an open-source platform for biological-image analysis. Nat Methods *9*, 676–682.

Schrode, N., Saiz, N., Di Talia, S., and Hadjantonakis, A.-K. (2014). GATA6 Levels Modulate Primitive EndodermCell Fate Choice and Timing in the Mouse Blastocyst. Dev Cell 1–14.

Shimosato, D., Shiki, M., and Niwa, H. (2007). Extra-embryonic endoderm cells derived from ES cells induced by GATA factors acquire the character of XEN cells. BMC Dev Biol *7*, 80.

Silva, J., Nichols, J., Theunissen, T.W., Guo, G., van Oosten, A.L., Barrandon, O., Wray, J., Yamanaka, S., Chambers, I., and Smith, A. (2009). Nanog is the gateway to the pluripotent ground state. Cell *138*, 722–737.

Skarnes, W.C., Rosen, B., West, A.P., Koutsourakis, M., Bushell, W., Iyer, V., Mujica, A.O., Thomas, M., Harrow, J., Cox, T., et al. (2011). A conditional knockout resource for the genome-wide study of mouse gene function. Nature *474*, 337–342.

Snoussi, E.H. (1998). Necessary Conditions for Multistationarity and Stable Periodicity. J. Biol. Syst. *06*, 3–9.

Thomas, R. (1981). On the Relation Between the Logical Structure of Systems and Their Ability to Generate Multiple Steady States or Sustained Oscillations. In Springer Series in Synergetics, J. Della Dora, J. Demongeot, and B. Lacolle, eds. (Berlin, Heidelberg: Springer Berlin Heidelberg), pp. 180–193–193.

Wang, Y., Smedberg, J.L., Cai, K.Q., Capo-Chichi, D.C., and Xu, X.-X. (2011). Ectopic expression of GATA6 bypasses requirement for Grb2 in primitive endoderm

formation. Dev Dyn *240*, 566–576.

Weintraub, H., Tapscott, S.J., Davis, R.L., Thayer, M.J., Adam, M.A., Lassar, A.B., and Miller, A.D. (1989). Activation of muscle-specific genes in pigment, nerve, fat, liver, and fibroblast cell lines by forced expression of MyoD. Proc Natl Acad Sci USA *86*, 5434–5438.

Yamanaka, Y., Lanner, F., and Rossant, J. (2010). FGF signal-dependent segregation of primitive endoderm and epiblast in the mouse blastocyst. Development *137*, 715–724.

Figures

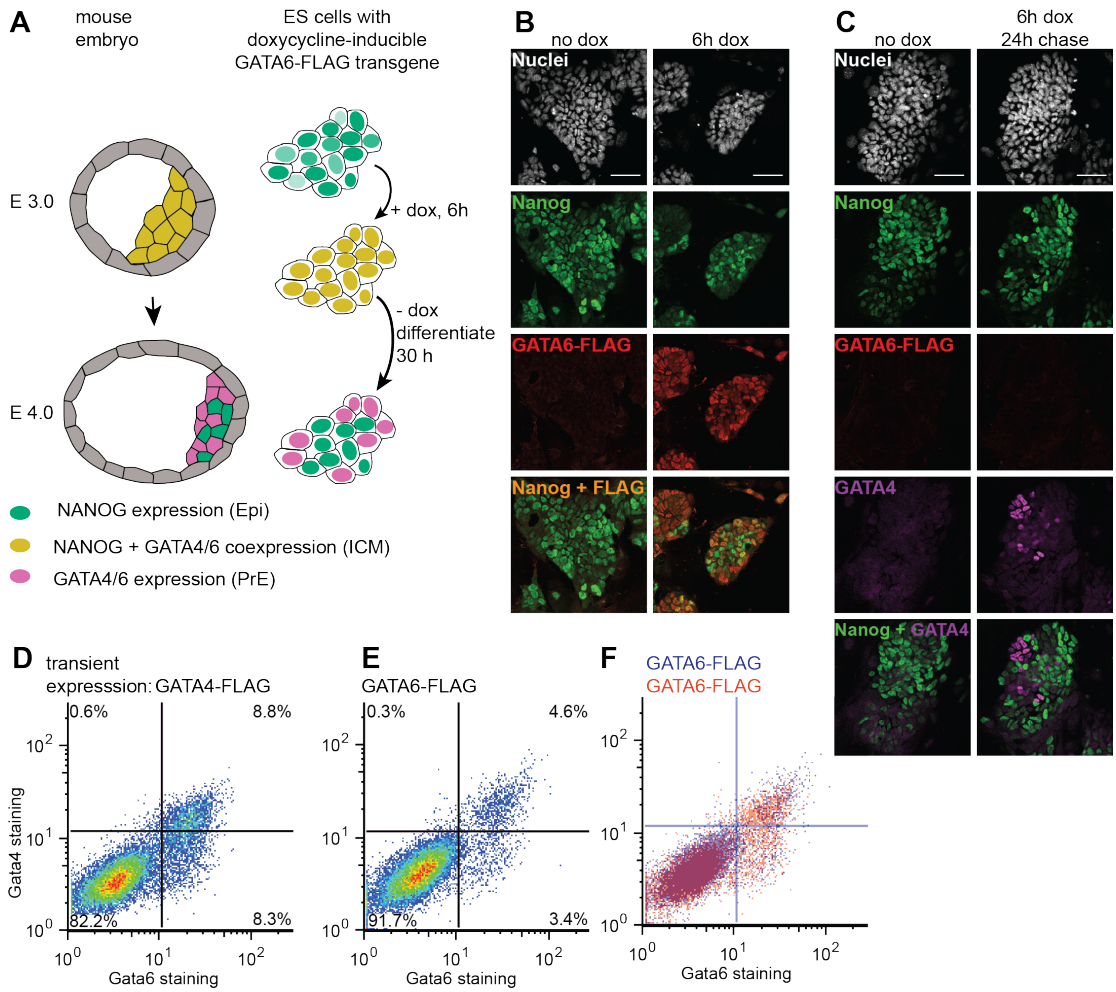

Figure 1: Expression of endogenous markers of extraembryonic endoderm differentiation following transient expression of GATA6-FLAG and GATA4-FLAG.

A Outline of the experimental approach. Addition of doxycycline to ES cells carrying a GATA6-FLAG transgene under a doxycycline-inducible promoter creates a GATA6/Nanog co-expression state similar to the situation in the ICM, from which cells can choose to differentiate along extraembryonic fates or return to the original Nanog-positive state. **B** Immunostaining of untreated (left) or dox-treated (right) inducible ES cells. Merge of Nanog and GATA6-FLAG stain indicates co-expression of the two proteins in individual cells after 6h of doxycycline treatment. Scale bar,

50 µm. **C** Immunostaining of inducible cell lines 24 h after the end of a 6 h doxycycline treatment. Expression of endogenous GATA4 protein is only detected after doxycycline treatment (right), and is mutually exclusive with Nanog expression. Scale bar, 50 µm. **D,E,F** Flow cytometric analysis of cells carrying an inducible GATA4-FLAG transgene (**D**) or an inducible GATA6-FLAG transgene (**E**) immunostained for GATA4 and GATA6 one day after a 6h doxycycline pulse. **F** shows the overlay of **D** and **E**. Inducible GATA4-FLAG and GATA6-FLAG expression results in the same pattern of endogenous GATA4 and GATA6 co-expression.

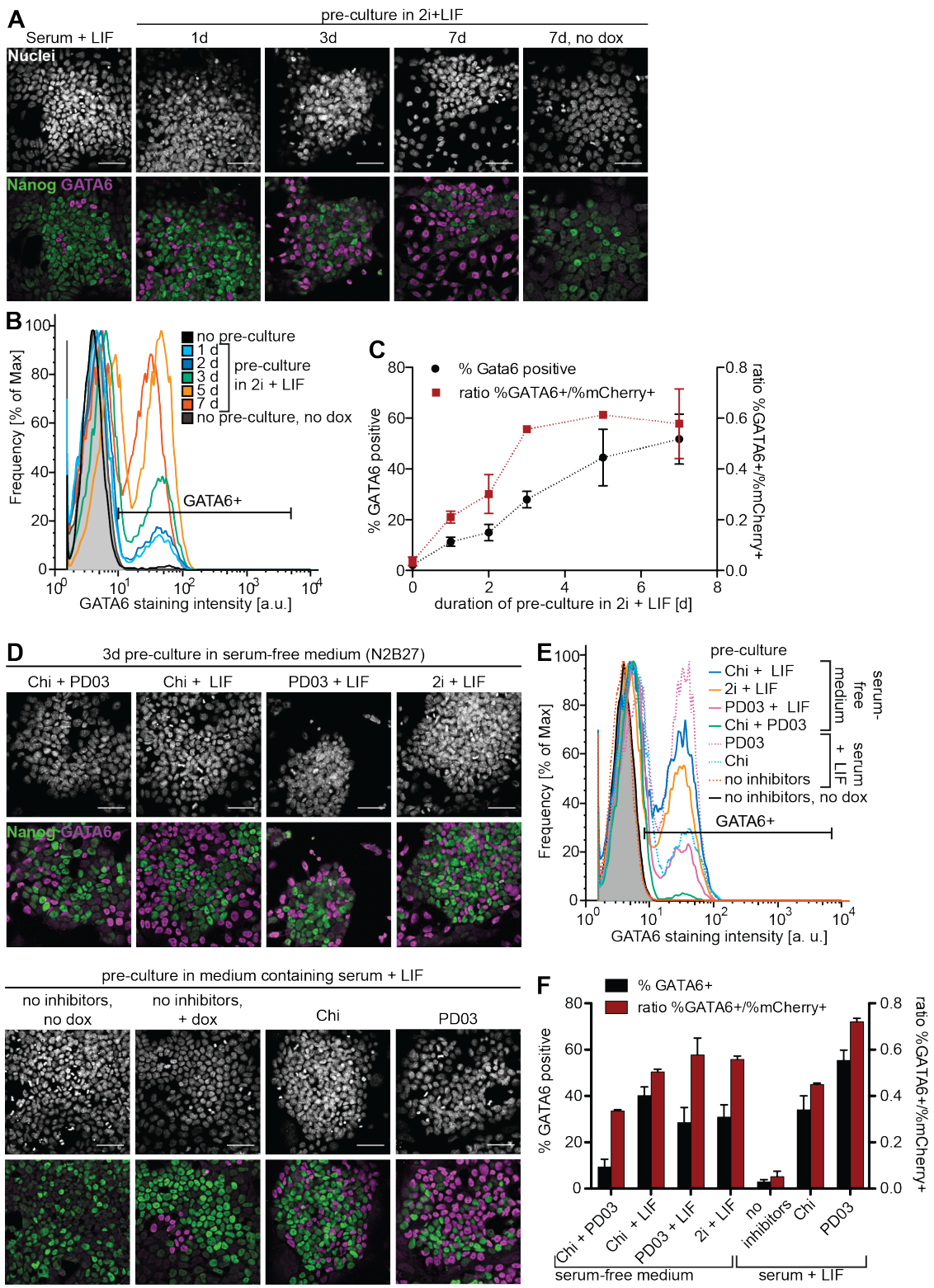

Figure 2: Culture conditions affect responsiveness to GATA4-mCherry expression.

A Immunostaining of GATA4-mCherry inducible ES cells cultured for increasing periods of time in 2i + LIF medium before a 6h doxycycline pulse followed by a 24h

chase in medium containing serum + LIF. Scale bars, 50 µm. **B** Flow cytometric analysis of cells treated as in **A** and stained for GATA6. **C** Average percentage of GATA6-positive cells (black) and ratio of the percentages of GATA6-positive and mCherry-positive cells (red) for different durations of pre-culture in 2i. Data averaged from 3 (% $GATA6^+$) or 2 (ratios) independent experiments, errors bars state standard deviation. **D** Immunostaining of GATA4-mCherry inducible ES cells cultured for 3d in the indicated media before a 6h doxycycline pulse followed by a 24h chase in medium containing serum + LIF. Scale bars, 50 µm. **E** Flow cytometric analysis of cells treated as in **D** stained for GATA6. **F** Average percentage of $GATA6^+$ cells (black) and ratio of the percentages of $GATA6^+$ and $mCherry^+$ cells (red) for different pre-culture media. Data averaged from 3 (% $GATA6^+$) or 2 (ratios) independent experiments, errors bars indicate standard deviation.

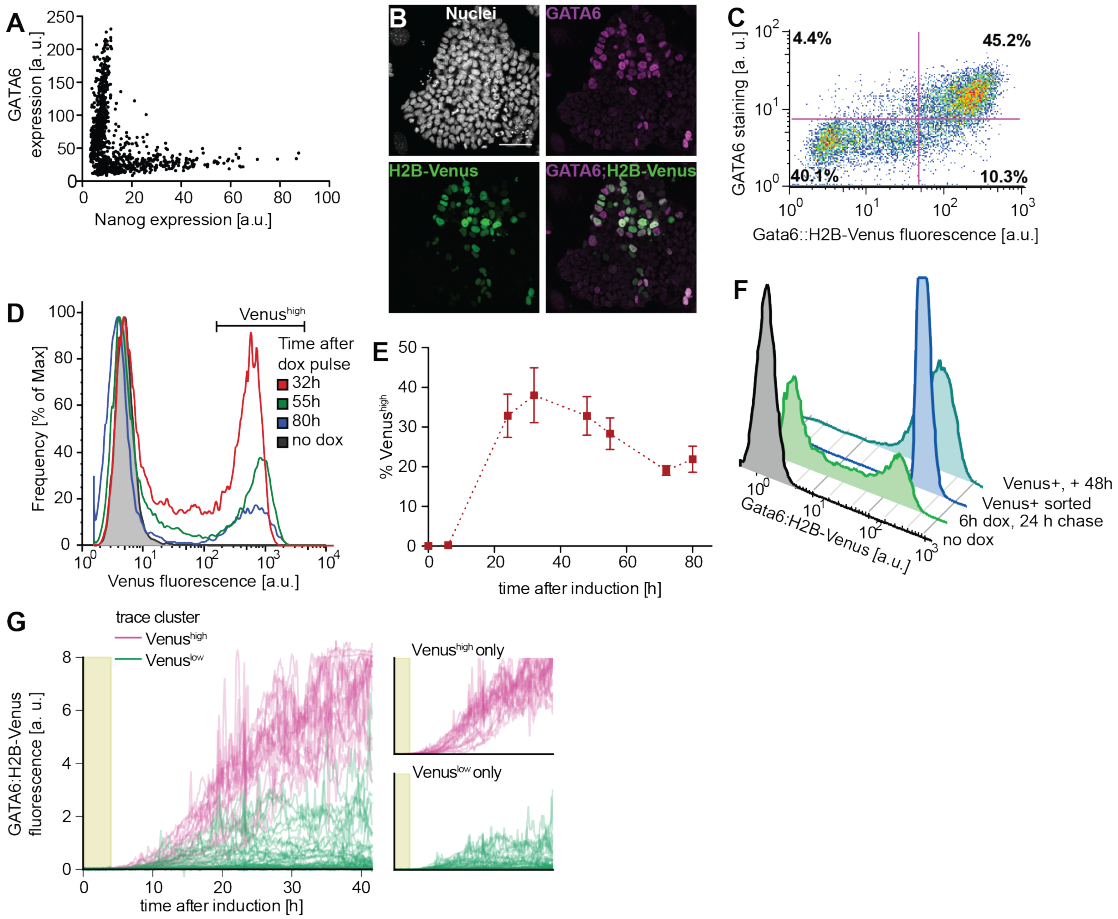

Figure 3: Transient GATA4-mCherry induces stable expression of PrE marker genes.

A Quantitative immunofluorescence analysis of cells stained for Nanog and GATA6 24h after a 6h doxycycline pulse. Each datapoint indicates relative staining intensity of a single cell. Expression of Nanog and GATA6 is mutually exclusive. **B** Immunostaining of ES cells carrying an inducible GATA4-mCherry transgene and a transcriptional H2B-Venus Gata6-reporter fixed 24h after a 6h doxycycline pulse. Reporter expression and expression of GATA6 overlap in individual cells. Scale bar, 50 µm. **C** Flow cytometric analysis of Gata6-reporter cells treated as in **B**. Cells with high Venus expression levels stain positive for endogenous GATA6 protein. **D** ES cells carrying an inducible GATA4-mCherry transgene and a transcriptional H2B-

Venus Gata6-reporter subjected to a 6h doxycycline pulse were analyzed at different time-points after the end of the pulse. Expression levels of cells in the Venus^{high}-peak do not change between 32h and 80 h after doxycycline addition. **E** Percentages of Venus^{high} cells at different times after a 6h doxycycline pulse. Data points represent mean ± standard deviation from three independent experiments. **F** Venus^{high} cells were flow sorted 18h after the end of a 6h doxycycline pulse (dark blue), cultured for 48h and analyzed for Venus expression. Venus expression levels of the Venus^{high} population are constant over this period, and no Venus^{negative} cells appear. **G** H2B-Venus fluorescence intensity values of individual Gata6-reporter cells tracked in time-lapse movies during and following a 6h doxycycline pulse (shaded area). Reporter expression can be detected from 8h after doxycycline addition onwards. Traces are color-coded according to hierarchical clustering based on H2B-Venus expression levels. Small panels on the right show traces for each cluster separately. See also Supplementary Figure S5 and Supplementary Movie S1.

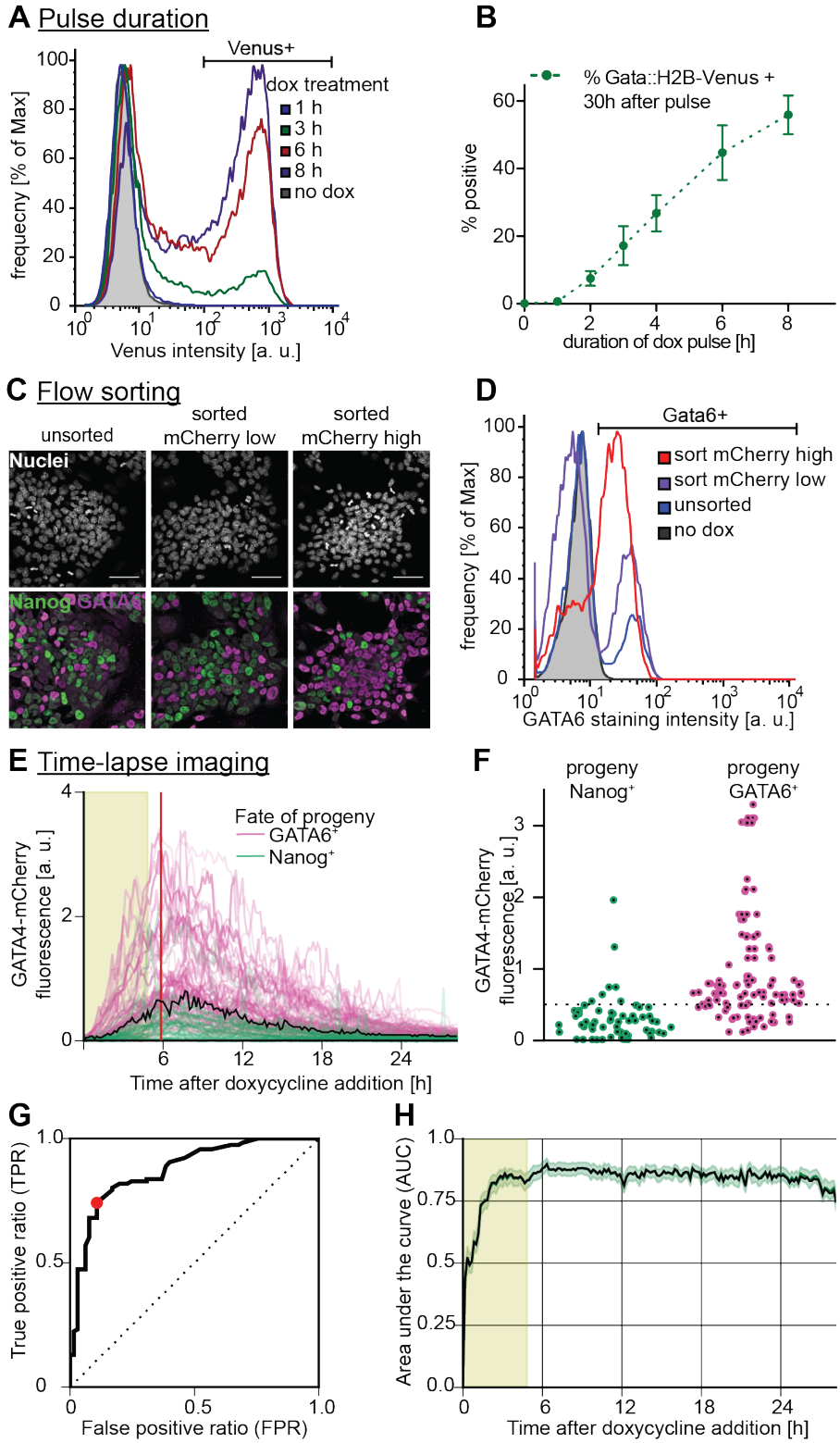

Figure 4: A GATA4-mCherry threshold dose determines PrE-like differentiation.

A Flow cytometric analysis of Venus fluorescence in cells carrying a doxycycline-inducible GATA4-mCherry transgene and a Gata6 transcriptional reporter one day

after doxycycline pulses of indicated lengths. The percentage of Venus^{high} cells increases with doxycycline pulse length. **B** Quantitative analysis of results from **A**. Data points show mean and standard deviation from three independent experiments. **C** Cells sorted for low (middle) and high (right) GATA4-mCherry expression levels after a 6h doxycycline pulse and immunostained 30h after re-plating. Unsorted control is on the left. Scale bar, 50 µm. **D** Flow cytometric analysis of cells treated as in **C** stained for GATA6 expression. A larger proportion of GATA4-mCherry^{high} cells activate GATA6 expression compared to GATA4-mCherry^{low} cells. **E** GATA4-mCherry fluorescence traces of cells filmed during and after a 6h doxycycline pulse. Cells were immunostained for Nanog and GATA6 expression after time-lapse imaging and individual traces are color-coded according to marker gene expression of a cell's pogeny at the end of the time-lapse. Area shaded in green indicates duration of doxycycline pulse, red bar indicates time point analyzed in **F**, **G**, and black curve indicates optimal threshold calculated by ROC. See also Supplementary movie S2 and Supplementary Figure S8. **F** GATA4-mCherry fluorescence intensity of cells from the experiment shown in **E** at a single time-point 1h after removal of doxycycline (red vertical line in **E)**. Optimal threshold to predict fate choice estimated by ROC analysis is indicated by a black line. **G** Receiver operating characteristics curve for the time-point shown in **F**. The optimal threshold maximizing the difference between the true positive and false positive prediction rate (TPR and FPR) is indicated by a red dot. **H** Area under the curve (AUC) values from ROC analysis in all time frames of the experiment shown in **E**. The AUC, a measure for the usefulness of GATA4-mCherry expression levels as predictor for GATA6 expression at the end of the time-lapse, increases quickly as GATA4-mCherry expression is induced. Error margin indicates standard deviation determined by bootstrapping.

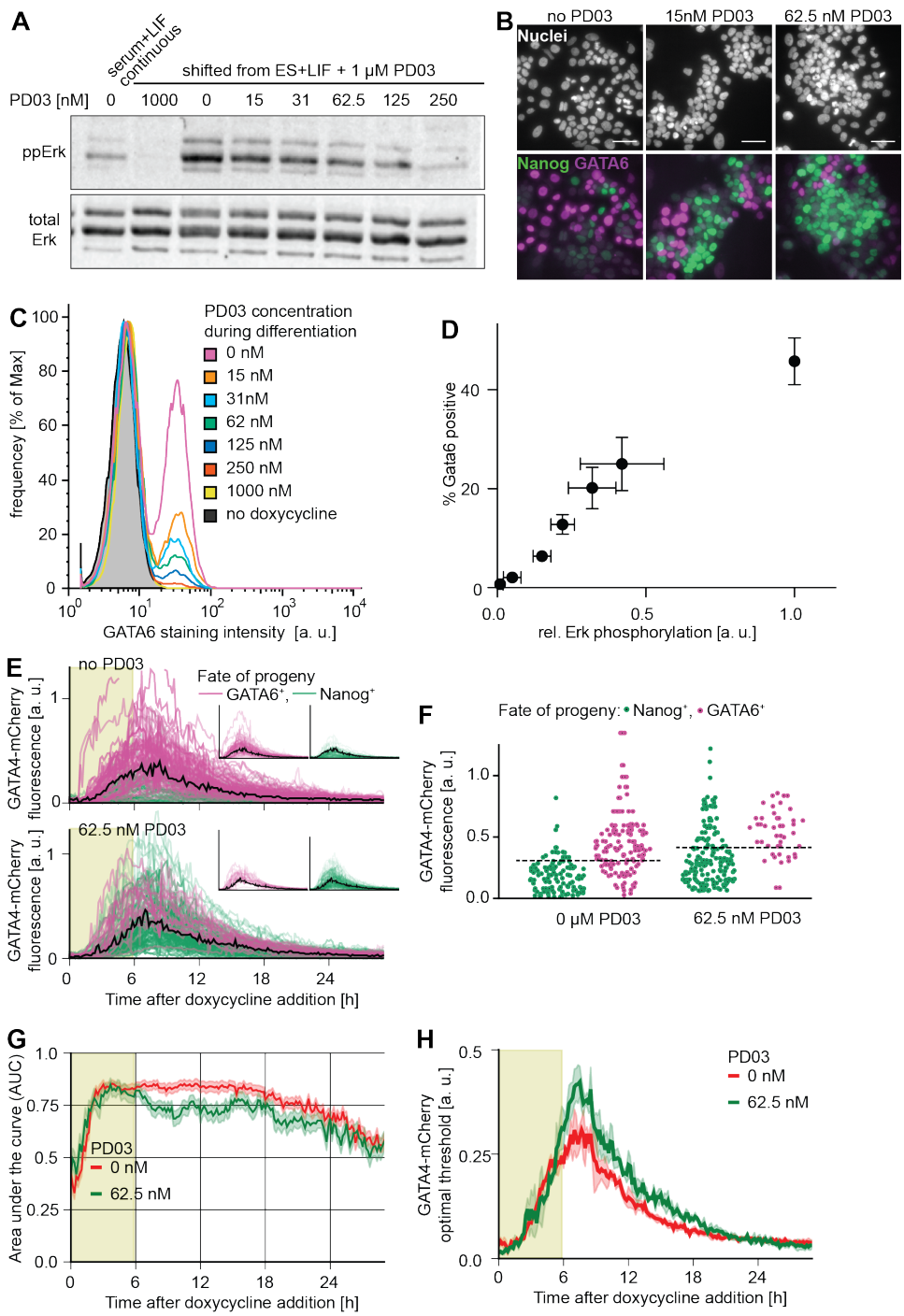

Figure 5: MAPK signaling controls the proportion of cells with PrE-like differentiation.

A Immunoblot detecting phosphorylated Erk (top panel) and total Erk (bottom panel) in ES cells grown for 3d in the presence of serum and 1µM PD03 1h after transfer into medium containing indicated amounts of PD03. **B** Immunostaing of ES cells

carrying an inducible GATA4-mCherry transgene after a 6h doxycycline pulse followed by 24h of differentiation in the indicated amounts of PD03. Increasing doses of the inhibitor reduce the number of GATA6-positive cells. Scale bar, 50 µm. **C** Flow cytometric analysis of GATA6 expression in cells treated as in **B**. **D** Plot of relative Erk phosphorylation levels determined by immunoblotting versus percentage of GATA6-positive cells for different concentrations of PD03. Shown are mean and standard deviation from at least three independent experiments per condition. **E** GATA4-mCherry fluorescence traces of cells filmed during and after a 6h doxycycline pulse in the absence PD03 (upper panel) or with 62.5 nM PD03. Cells were immunostained for Nanog and GATA6 expression after time-lapse imaging and individual traces are color-coded according to marker gene expression of a cell's progeny at the end of the time-lapse. Shaded area indicates presence of doxycycline, black trace indicates optimal threshold estimated by ROC, and insets show traces for cells with GATA6- and Nanog-positive progeny separately. **F** GATA4-mCherry fluorescence intensity of cells from the experiment shown in **E** at a single time-point 1h after removal of doxycycline in the absence of PD03 (left) and in 62.5 nM PD03 (right). Presence of 62.5 nM PD03 shifts the distribution of GATA4-mCherry expression levels in both the differentiating and non-differentiating cohort. **G** Area Under the Curve (AUC) from ROC analysis for each time point of the dataset shown in **E** and **F** for no PD03 (red) and 62.5 nM PD03 (green). Fate choice can be predicted from GATA4-mCherry expression levels with similar confidence in both conditions from 3h after addition of doxycycline. The decrease of the curves after approx. 20h is due to the very low levels of GATA4-mCherry expression at this time. Error margin indicates standard deviation determined by bootstrapping (n=1000). **H** Optimal threshold values to predict differentiation at the end of the time-lapse from GATA4-

mCherry expression in the absence of PD03 (red) and in the presence of 62.5 nM PD03 (green). The optimal threshold increases with decreasing MAPK signaling. Error margins indicate standard deviation determined from bootstrapping (n=1000).

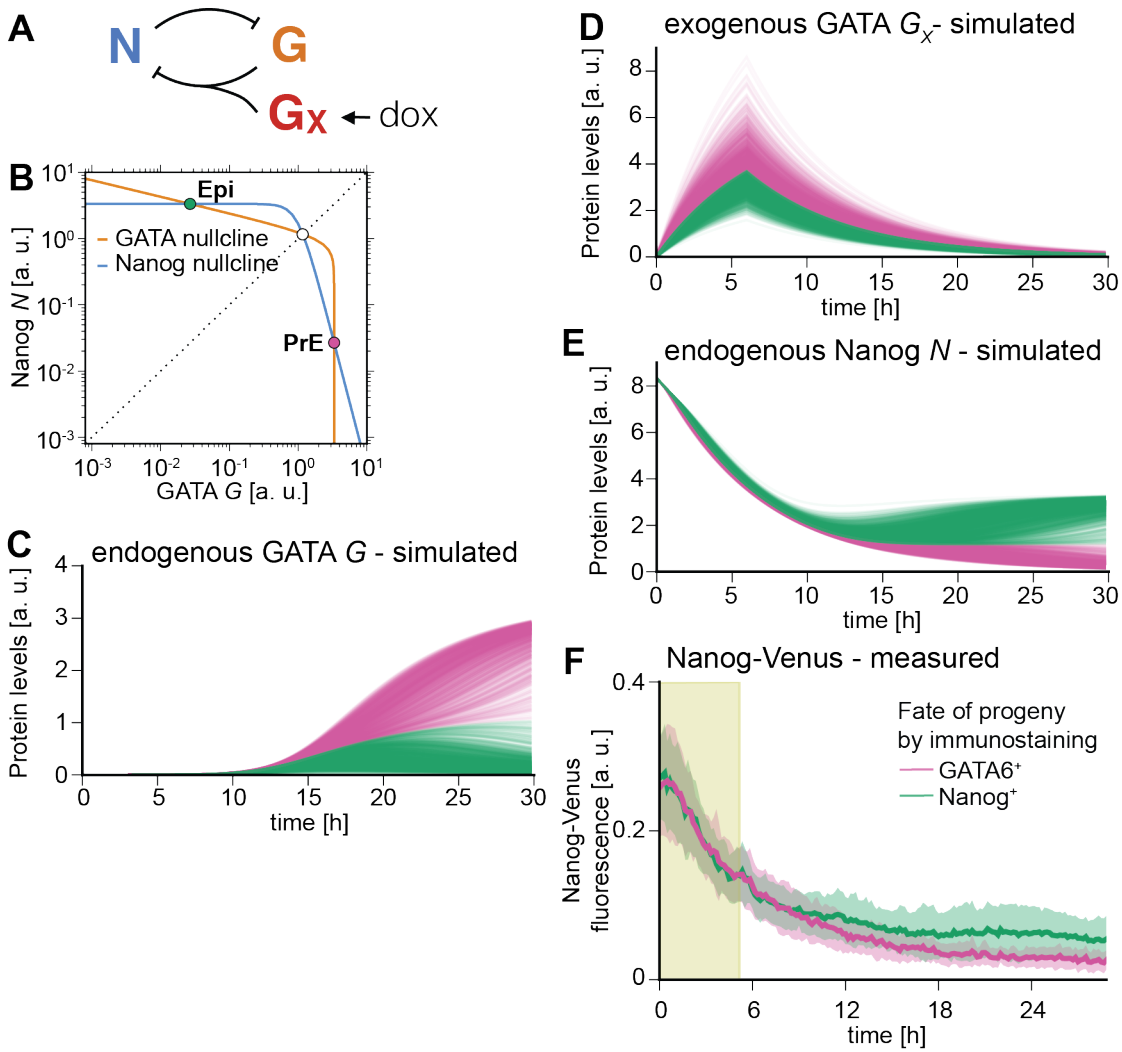

Figure 6: A simple mutual repression circuit recapitulates experimentally observed expression dynamics.

A Connectivity of the mutual repression circuit used in dynamic simulations. **B** Phase portrait depicting the autonomous dynamics of the system in **A**. The Nanog nullcline (blue line) and the GATA nullcline (orange line) cross thrice, creating three steady states in the system, two of which are stable. A separatrix (dashed line) separates combinations of Nanog and GATA expression evolving into the Nanog^{high}, GATA^{low} stable state corresponding tot the Epi fate (green dot) from those that evolve into the Nanog^{low}, GATA^{high} PrE state (purple). **C**, **D**, **E** Simulated time traces of endogenous GATA *G* (**C**) exogenous GATA4-mCherry G_X (**D**), and Nanog expression (**E**). Traces eventually reaching high and low GATA expression levels in **C** are color coded in

purple and green, respectively, and corresponding traces have same color in **C**, **D** and **E**. A defined threshold of Gx expression separates cells that eventually will express high levels of endogenous GATA from those where endogenous GATA expression is transient and low. **F** Average Nanog-Venus expression levels in cells carrying a Nanog-Venus translational reporter and an inducible GATA4-mCherry transgene during and following a 6h doxycycline pulse. Cells were classified into GATA6-positive and Nanog-positive by immunostaining after the time-lapse. Presence of doxycycline indicated by light green rectangle. Lines and shaded areas indicate mean Nanog-Venus fluorescence levels and standard deviation of ancestors of Nanog^{+} cells in green and GATA6^{+} cells in purple. See also Supplementary Movie S3.

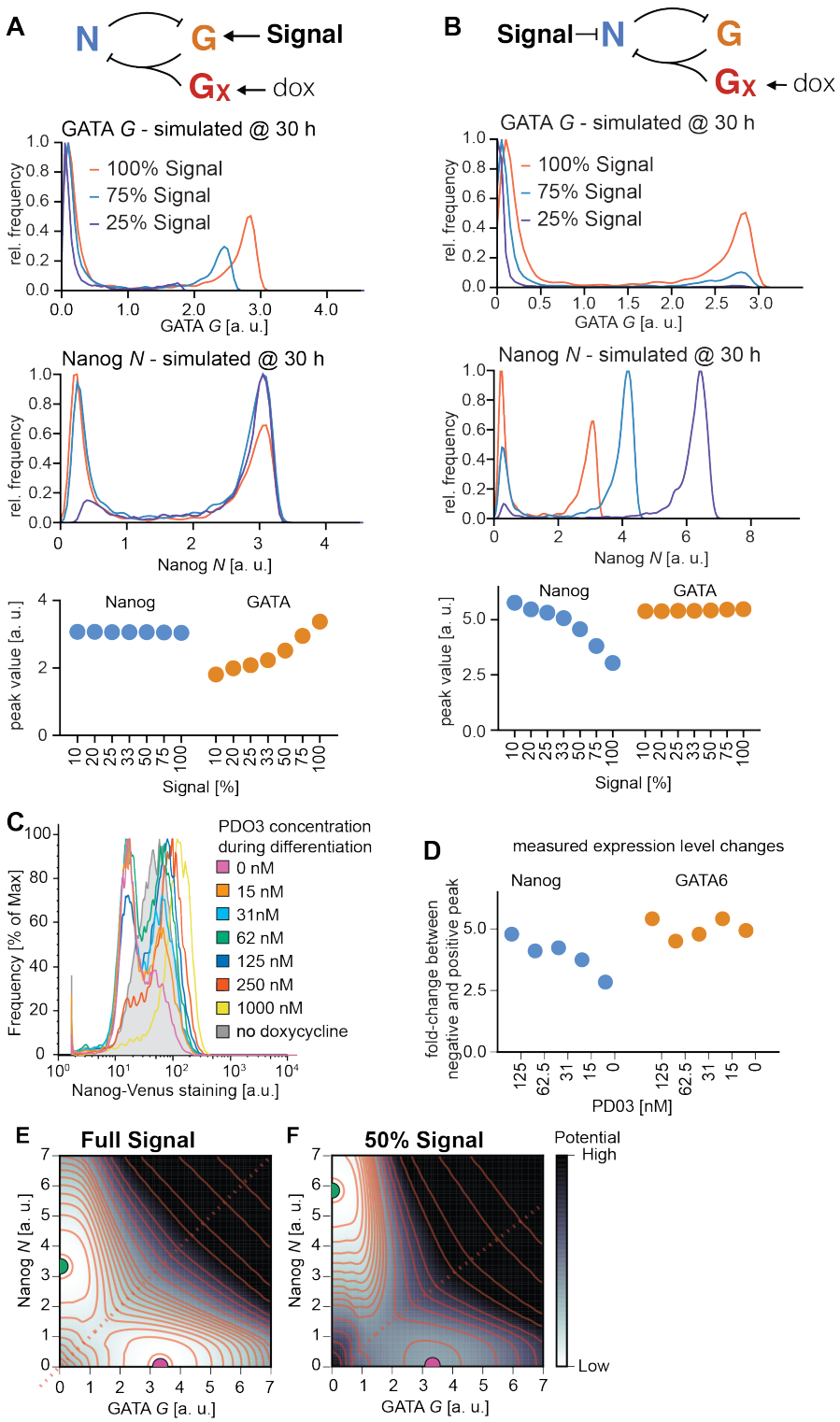

Figure 7: MAPK signaling controls the proportion of PrE-like cells through inhibition of the Epi program.

A, B Upper panels: Schematic representation of the modes of signaling interactions tested in the model; **A**: signaling promotes GATA production, **B**: Signaling inhibits

Nanog production. Middle panels: Simulated histograms and location of histogram peaks for endogenous GATA *G* and Nanog *N* expression levels after 30h in populations of 2000 cells at varying signaling levels. Reducing signaling levels decreases the fraction of GATA-positive cells and increases the fraction of Nanog-positive cells in both circuits, but expression levels in the positive population depend on the type of MAPK signaling input into the system. **C** Flow cytometric analysis of Nanog-Venus expression 30h after a 6h doxycycline pulse. Staining intensity of the left, Venus-negative peak is constant, whereas staining intensity of the right peak changes with the PD03 concentration during the experiment. **D** Relative change of the Nanog-Venus-positive (blue) and GATA6-positive (orange) peak compared to the negative peak estimated from the flow cytometry experiments in **C** (Nanog-Venus) and Fig. 5 **C** (GATA6) for different concentrations of PD03. See Supplementary Figure S11 for details on estimation of peak positions. The relative position of the Nanog-Venus-positive peak shifts towards higher expression levels at higher concentrations of PD03, whereas no clear trend can be observed for GATA6 expression levels. **E**, **F** Quasi-Potentials derived from the autonomous dynamics of the system in **B** for two different signaling levels. Darker regions have higher potential, i.e. stronger dynamic changes of the transcription factor concentrations. Solid orange lines indicate levels of the same potential, dashed orange line indicates the separatrix (ridge) that separates the basins of attraction corresponding to the $Nanog^{high}$, $GATA^{low}$ state (green dot) representing the embryonic Epi fate and the $Nanog^{low}$, $GATA^{high}$ state (purple dot) representing the extraembryonic fate. Lowered signaling (**F**) bends the separatrix and increases the size of the basin of attraction corresponding to the Epi fate relative to that of the basin of attraction of the PrE fate.

Supplementary Material

Supplementary Figures

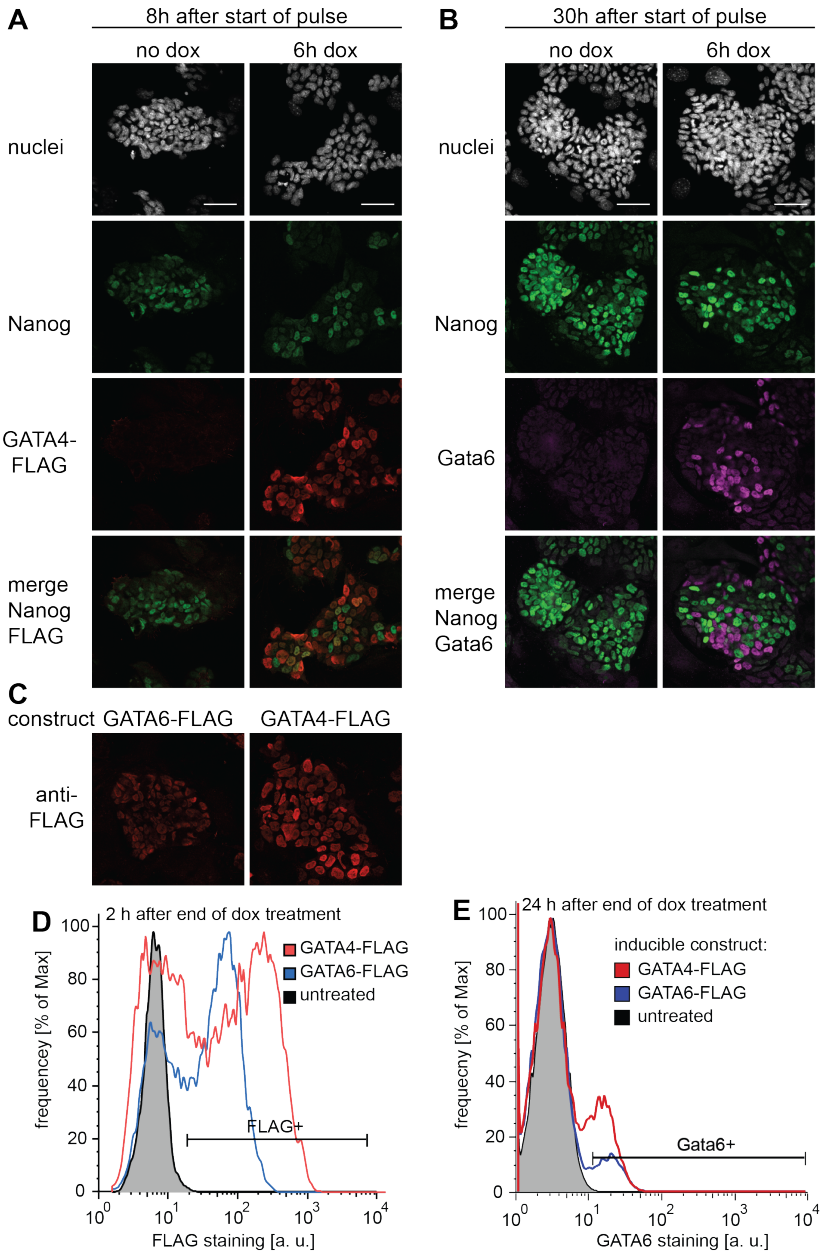

F

construct	% FLAG+ 2 h after end of treatment	mean fluorescence intensity of FLAG staining	% GATA6+ 24h after end of treatment
GATA4-FLAG	53.5 ± 7.7 (N = 3)	159.7 ± 26.1 (N = 3)	16.5 ± 2.6 (N = 3)
GATA6-FLAG	47.4 ± 7.1 (N = 3)	63.9 ± 11.8 (N = 3)	8.9 ± 1.2 (N = 3)

Supplementary Figure S1: Inducible GATA4-FLAG reaches higher expression levels and triggers PrE-like differentiation in a larger proportion of cells compared to GATA6-FLAG.

A, B Immunostaining of ES cells carrying a doxycycline-inducible GATA4-FLAG transgene 2 h (**A**) or 24 h (**B**) after a 6h treatment with doxycycline. Untreated controls are on the left. Exogenous GATA4-FLAG is co-expressed with Nanog shortly after the treatment, but degraded one day later. Endogenous GATA6 is expressed one day after the treatment in a mutually exclusive pattern with Nanog. Scale bar, 50 μm. **C**, **D** Comparison of GATA6-FLAG and GATA4-FLAG transgene induction efficiency. Cells were immunostained for FLAG 2 h after a 6 h doxycycline pulse and analysed by confocal microscopy (**C**) or flow cytometry (**D**). The percentage of expressing cells is comparable between the two constructs, but GATA4-FLAG is expressed at higher levels in individual cells. One representative clone shown. **E** Flow cytometric analysis of cells immunostained for GATA6 24 h after transient expression of GATA4-FLAG (red) or GATA6-FLAG (blue). Inducible GATA4-FLAG expression triggers endogenous GATA6 expression in a larger proportion of cells compared to inducible GATA6-FLAG expression. One representative clone shown. **F** Quantitation of results from **D** and **E**; numbers state mean and standard deviation from three independent clones.

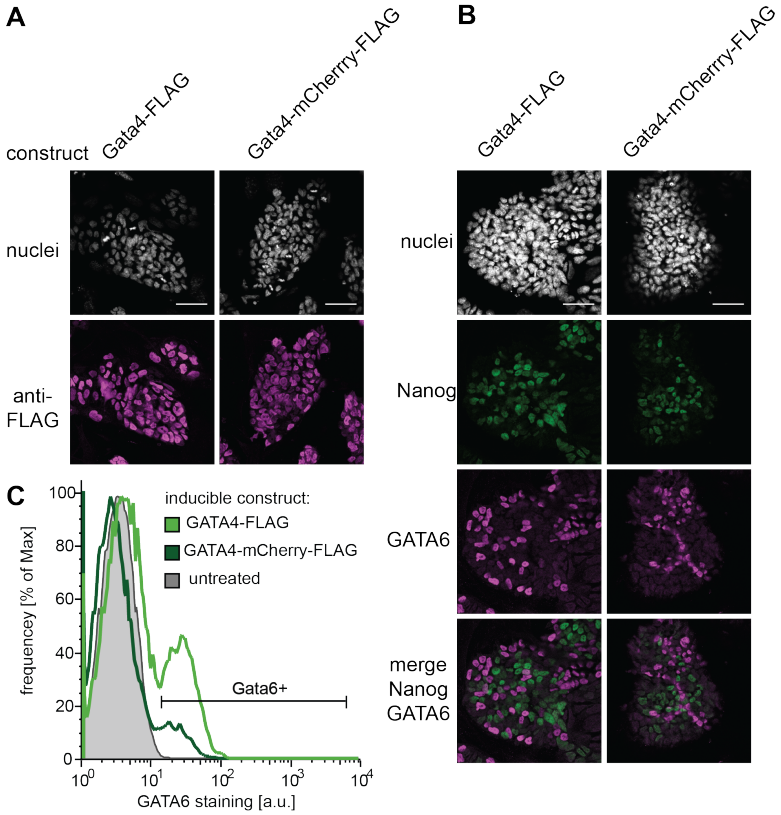

Supplementary Figure S2: Transient expression of GATA4-mCherry-FLAG can induce endogenous GATA6 expression.

A Immunostaining for FLAG in cells expressing GATA4-FLAG (left) or GATA4-mCherry-FLAG (right) following 6h of doxycycline treatment. Both inducible proteins are expressed in a comparable proportion of cells, but FLAG staining intensity is slightly lower for the mCherry-tagged protein, suggesting lower expression levels in individual cells. **B** Immunostaining for Nanog and GATA6 of cells carrying a GATA4-FLAG (left) or GATA4-mCherry-FLAG (right) transgene under doxycycline control 24h after a 6h treatment with doxycycline. Scale bars in **A**, **B**, 50 µm. **C** Flow cytometric analysis of cells treated as in **B** stained for GATA6 expression. GATA6 expression levels do not depend on the inducible protein used, but GATA4-mCherry FLAG induces expression of endogenous GATA6 in a smaller proportion of cells than GATA4-FLAG, possibly as a consequence of lower GATA4-mCherry expression levels in individual cells.

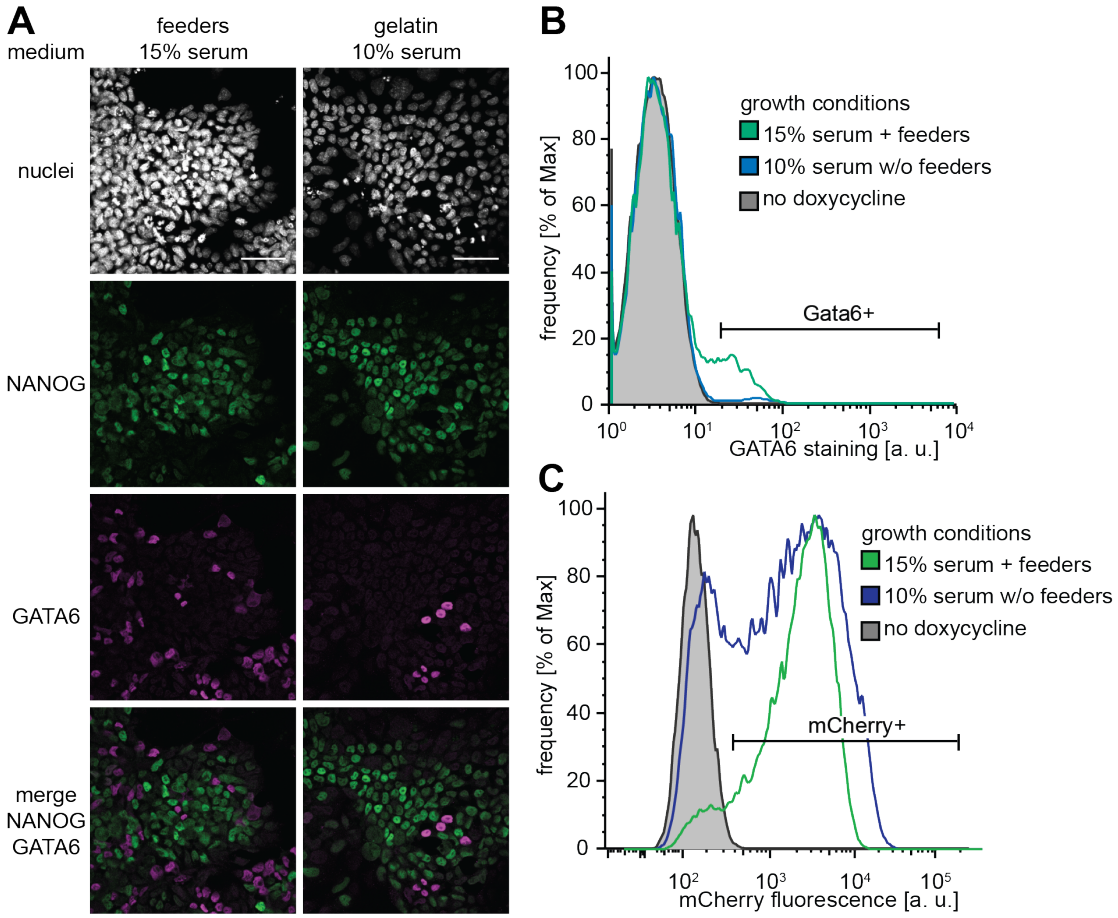

Supplementary Figure S3: Removal of feeders and reduction of serum levels reduces the accessibility of the PrE-like differentiation program.

A Immunostaing of cells carrying an inducible GATA4-mCherry transgene cultured on feeder cells in the presence of 15% serum (left) or in the absence of feeders in 10% serum (right) 24h after a 6h doxycycline pulse. Scale bar, 50 µm **B** Flow cytometric analysis of cells treated as in **A** and stained for GATA6. The proportion of GATA6-positive cells is severely reduced in the absence of feeders and lowered serum concentrations. **C** Flow cytometric analysis of GATA4-mCherry expression in cells treated as in **A** 2h after the end of the doxycycline treatment. Both conditions give robust expression of the inducible GATA4-mCherry protein.

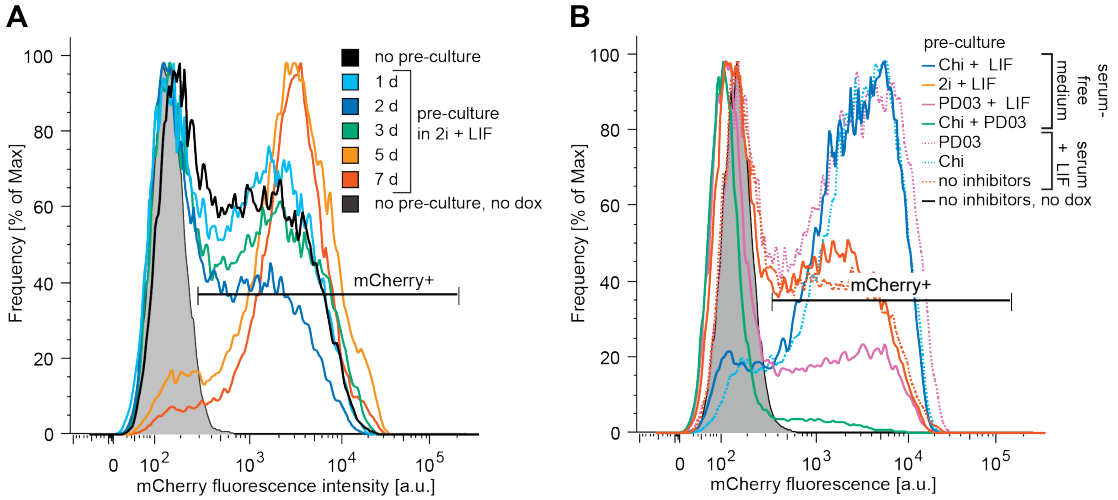

Supplementary Figure S4: Pre-culture regimes and –times affect the expression efficiency of the doxycycline-inducible transgene.

Cells grown for increasing periods of time in 2i + LIF medium (**A**) or cultured for 3d in the indicated media (**B**) were changed to medium containing serum + LIF and doxycycline, followed by flow cytometric analysis for GATA4-mCherry expression 2h after the end of a 6h doxycycline pulse.

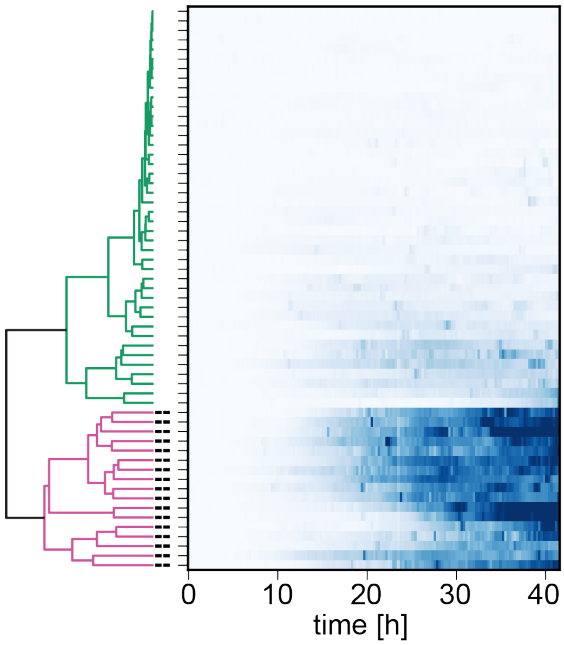

Supplementary Figure S5: Hierarchical clustering distinguishes groups of cells with high and low H2B-Venus expression in the Gata6 reporter line.

Gata6:H2B-Venus reporter cells were hierarchically clustered according to H2B fluorescence intensity values recorded during and after a 6h doxycycline pulse. Dark blue indicates strong fluorescence. This analysis identifies two main groups that markedly differ in their H2B-Venus expression intensity in the second half of the experiment. These two groups are highlighted by different branch colors (green: H2B-Venus^{low}, purple: H2B-Venus^{high}), and inform the color code in Fig. 3G; see also Supplementary movie S1.

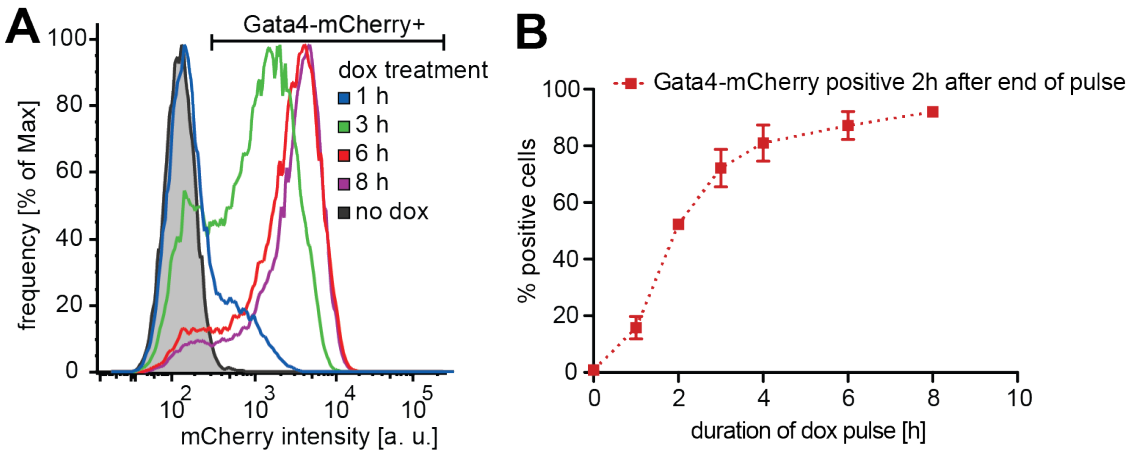

Supplementary Figure S6: Titration of GATA4-mCherry exposure by changing doxycycline pulse-length.

A Flow cytometric analysis of GATA4-mCherry expression in cells 2h after the end of doxycycline pulses of indicated duration. **B** Quantification of results from **A**. Datapoints represent mean ± standard deviation from three independent experiments.

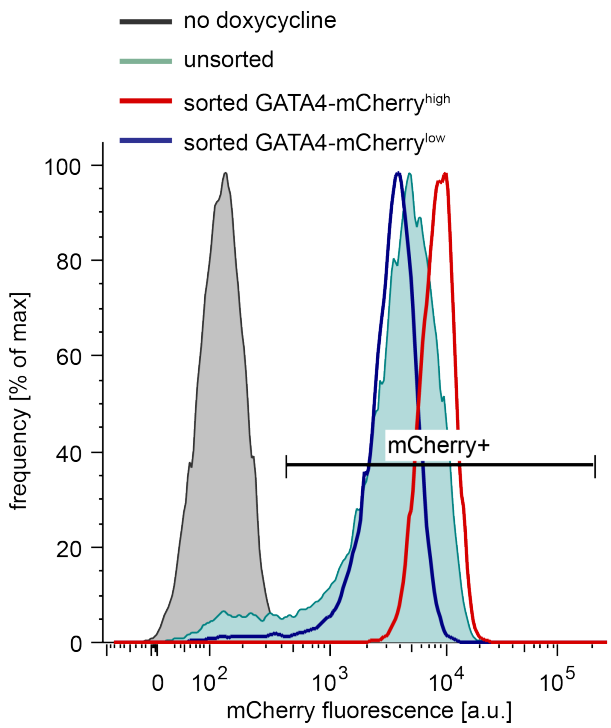

Supplementary Figure S7: Separation of GATA4-mCherry^{high} and GATA4-mCherry^{low} cells by flow cytometry.

Cells carrying a doxycycline-inducible GATA4-mCherry transgene were stimulated with doxycycline for 6h, trypsinised and sorted into two fractions according to mCherry fluorescence intensity. Figure shows the result of post-sort control, where fractions were analyzed on a separate cytometer approx. 2h after the end of the sort for fluorescence levels and purity. GATA4-mCherry^{high} population is in red, GATA4-mCherry^{low} population is in blue, unsorted cells are in shaded in turquoise, and uninduced control is shaded in grey.

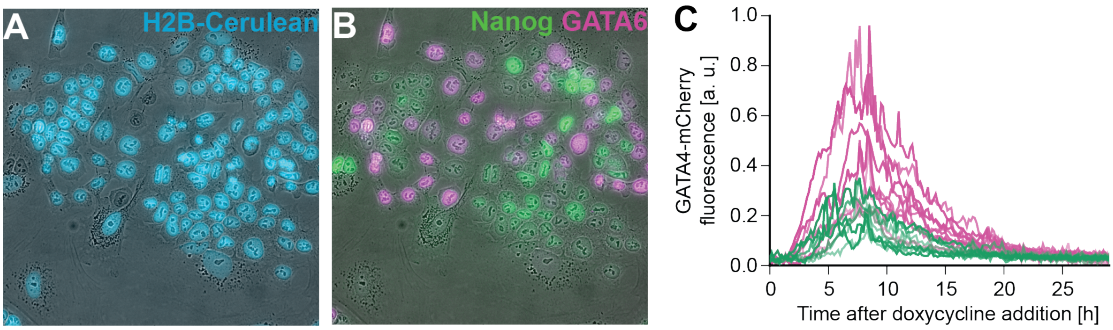

Supplementary Figure S8: Immunostaining of filmed cells for correlating GATA4-mCherry expression levels with fate choice.

A Overlay of brightfield and Cerulean fluorescence (blue) and **B** overlay of brightfield and immunostaining for Nanog (green) and GATA6 (purple) in cells carrying an inducible GATA4-mCherry transgene that had been filmed for 30h during and after a doxycycline pulse. **C** Individual GATA4-mCherry fluorescence traces recorded from cells shown in Supplementary Movie S2 and panels **A**, **B**, color-coded according to staining detected in **B**. Cells without clear GATA6 or Nanog immunostaining are not shown in **C**.

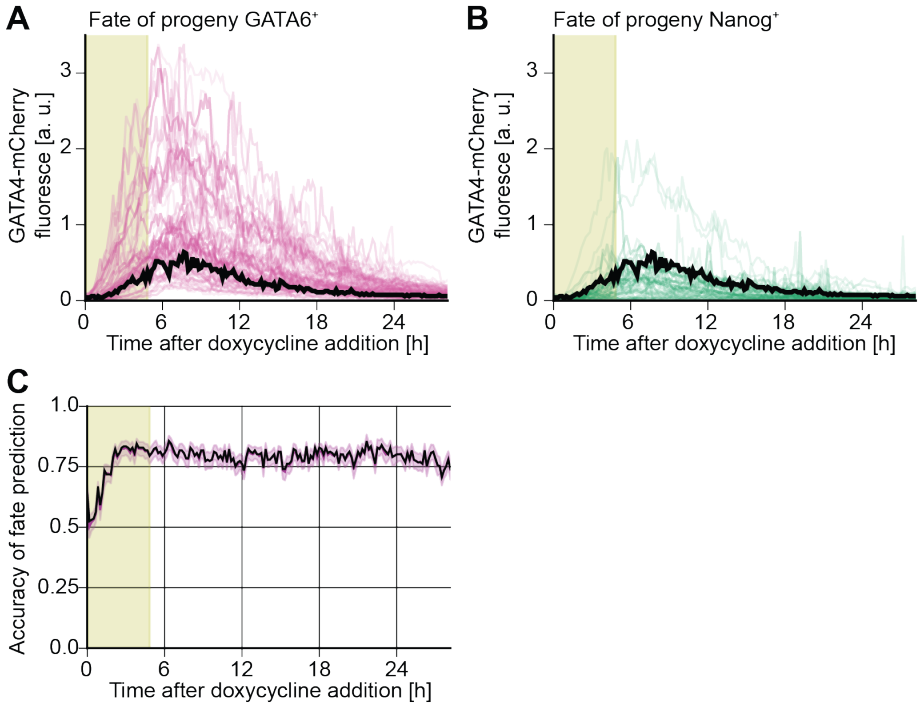

Supplementary Figure S9: Identification of an optimal threshold to predict fate choice from GATA4-mCherry expression levels.

A, **B** Fluorescence time traces of individual cells carrying an inducible GATA4-mCherry transgene filmed during and after a 6h doxycycline pulse. Cells with GATA6-positive progeny are depicted with purple traces in **A**, cells with Nanog-positive progeny are depicted with green traces in **B**. The optimal threshold detected by ROC analysis (Fig. 4G) is shown in black. **C** Accuracy of fate prediction using GATA4-mCherry fluorescence and optimal threshold depicted in **A**, **B**. Fate choice can be predicted with approx. 80% accuracy approx. 3h after addition of doxycycline. Area shaded in green indicates presence of doxycycline, area shaded in purple indicates standard deviation determined by bootstrapping.

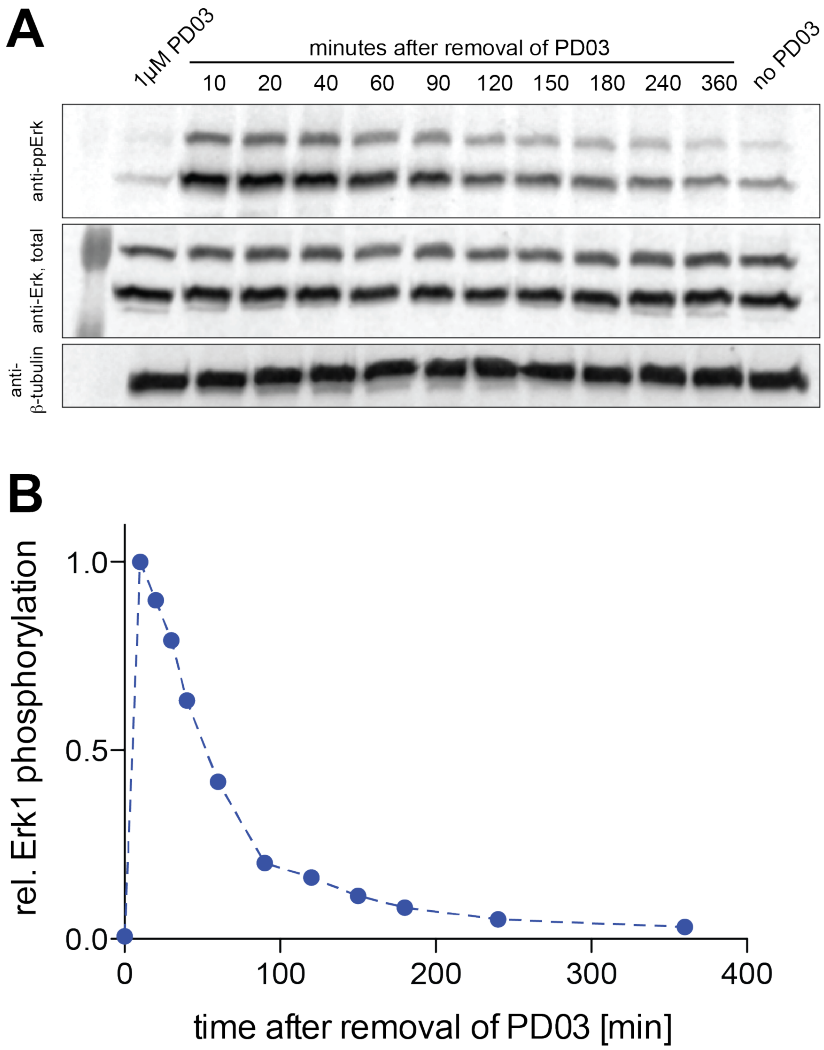

Supplementary Figure S10: Erk phosphorylation peaks transiently after removal of PD03.

A Immunoblot detecting phosphorylated Erk (top), total Erk (middle) and β-tubulin (bottom) in cells grown for 3d in the presence of 1µM PD03 following transfer into inhibitor-free medium for increasing periods of time. Removal of the inhibitor leads to rapid but transient phosphorylation of Erk. **B** Quantification of results from **A**. Signal intensity of phosphorylated p42 Erk were quantified and normalized by the signal intensity of the corresponding total p42 Erk band.

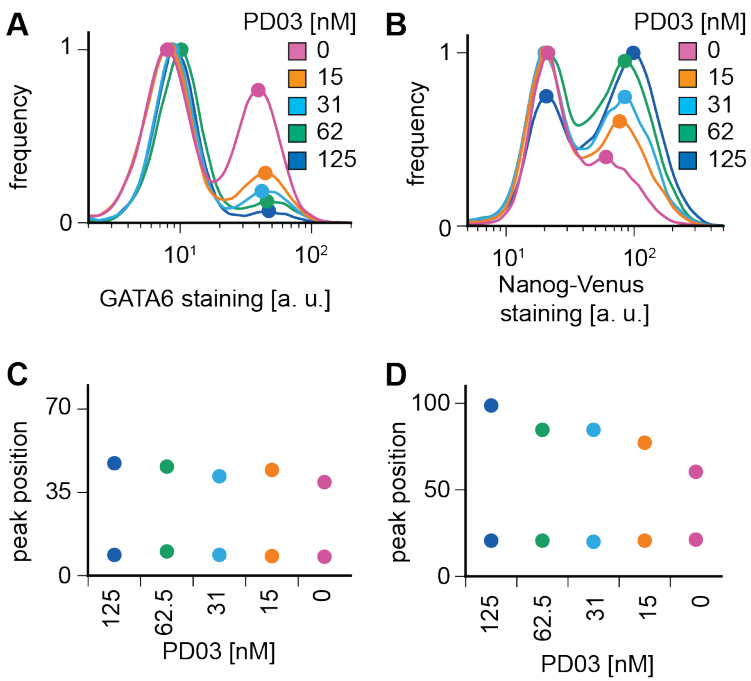

Supplementary Figure S11: Estimation of peak positions from flow cytometry data.

A, **B** Smoothened flow cytometry data from Figure 5 C (GATA6 staining, **A**) and Fig. 7 C (Nanog-Venus staining, **B**) with peak positions indicated by dots. Histograms were smoothened by transforming each bin of the original data into a gaussian distribution of values around the center of the bin, and peaks were identified as local maxima in the smoothened distributions. **C**, **D** Peak positions identified in **A**, **B** plotted for different PD03 concentrations. The position of the peak with low staining levels comprising of GATA6-negative and Nanog-Venus-negative cells is constant for different PD03-concentrations, whereas the position of the Nanog-Venus-positive, but not the GATA6-positive peak, changes with signaling levels.

1 **Supplementary Table S1**

2

Param.	Value	Units	Description
α_{N0}	½	*adimensional concentration units/h*	Maximum Nanog production rate in 100% signaling conditions.
α_{N1}	¾	*adimensional concentration units/h*	Increase in the max. Nanog production rate in 0% signaling conditions.
α_{G0}	½	*adimensional concentration units/h*	Maximum endogenous Gata production rate.
α_{G1}	½	*adimensional concentration units/h*	Maximum endogenous Gata production rate.
λ_N	*0.15*	*1/h*	Nanog protein degradation rate.
λ_G	*0.15*	*1/h*	Gata protein degradation rate.
p	*4*	-	Hill coefficient for the inhibition of Nanog by Gata.
q	*4*	-	Hill coefficient for the inhibition of Gata by Nanog.
σ_D	*0.25*	*adimensional concentration units/h*	Scale parameter of the lognormal distribution of the maximum production rate of exogenous Gata in the presence of doxycycline.
τ	*6*	*h*	Doxycycline pulse duration

3 *Supplementary Table S1. Parameter values of the model.*

4

Supplementary Movies

Supplementary Movie S1: Gata6:H2B-Venus expression dynamics following transient doxycycline treatment.

ES cells carrying the inducible GATA4-mCherry transgene, the transcriptional Gata6:H2B-Venus reporter and a randomly integrated H2B-Cerulean transgene under the control of the CAGS promoter were filmed during and after a 6h doxycycline pulse. Left panel shows overlay of brightfield image and Gata6:H2B-Venus fluorescence, left panel shows overlay of brightfield image and H2B-Cerulean fluorescence. Cell tracking is indicated by yellow circles (Venus channel) or yellow dots (Cerulean channel). See also Fig. 3G, Supplementary Figure S5.

Supplementary Movie S2: Tracking of GATA4-mCherry expression levels following transient doxycycline treatment

ES cells carrying a GATA4-mCherry transgene and a randomly integrated H2B-Cerulean transgene under the control of the CAGS promoter were filmed during and after a 6h doxycycline pulse. Left panel shows overlay of brightfield image and GATA4-mCherry fluorescence, left panel shows overlay of brightfield image and H2B-Cerulean fluorescence. Cell tracking is indicated by yellow circles (mCherry channel) or yellow dots (Cerulean channel). See also Fig. 4, Supplementary Figure S8.

Supplementary Movie S3: Nanog-Venus expression dynamics following transient doxycycline treatment

Time-lapse movie of ES cells carrying a randomly integrated H2B-Cerulean transgene under the control of the CAGS promoter (blue, upper left, overlay with brighfield image), the inducible GATA4-mCherry transgene (red, upper right), and a Nanog-Venus translational reporter (green, lower left) during and after a 6h doxycycline pulse. Lower right shows overlay of brightfield, GATA4-mCherry and Nanog-Venus fluorescence. Cell tracking is indicated by yellow dots and circles. See also Figure 6E.